Coordination Chemistry Reviews 255 (2011) 717–736

Contents lists available at ScienceDirect

Coordination Chemistry Reviews

journal homepage: www.elsevier.com/locate/ccr

Review

Coordination chemistry of corroles with focus on main group elements

Iris Aviv-Harel, Zeev Gross*

Schulich Faculty of Chemistry, Technion - Israel Institute of Technology, Haifa 32000, Israel

Contents

ARTICLE INFO

Article history:
Received 30 June 2010
Accepted 25 September 2010
Available online 7 October 2010

This contribution is dedicated to the occasion of the 75th birthday of Harry Gray, a brilliant scientist, close friend, wonderful collaborator and, most important of all, a true *mentsh* (person of integrity and honor).

ABSTRACT

The discovery of facile methodologies for the synthesis of triarylcorroles initiated extensive research on the corresponding metal complexes, ranging from elucidation of their fundamental physical properties to utilization of their chemical reactivity for many applications. This review focuses on the coordination chemistry of main group elements chelated by tetradentate and trianionic 5,10,15-triarylcorroles, which led to the elucidation of unique photophysical, crystallographic and electrochemical characteristics of these complexes. The facile access to a variety of complexes in which these and other properties can

Abbreviations: tpfc, 5,10,15-trispentafluorophenyl corrole; tpc, 5,10,15-triphenylcorrole; bstpfc, 2,17-bis-sulfonato-5,10,15-(tpfc); oec, 2,3,7,8,12,13,17,18-octaethylcorrole; thfpc, 5,10,15-tris(heptafluoropropyl)corrole; tdcc, 5,10,15-tris(2,6-dichlorophenyl)corrole; ttc, 5,10,15-tri-p-tolylcorrole; T(4-Me-P)C, 5,10,15-tris(4-methylphenyl)corrole; T(4-CF_3-P)C, 5,10,15-tris[(4-trifluoromethyl)phenyl]corrole; N3, cis-bis(4,4′-dicarboxy-2,2′-bipyridine)dithiocyanato ruthenium(II); A, absorbance.

* Corresponding author. Fax: +972 4829 5703.
E-mail address: chr10zg@tx.technion.ac.il (Z. Gross).

0010-8545/$ – see front matter
doi:10.1016/j.ccr.2010.09.013

Keywords:
Corroles
Zinc
Gallium
Aluminum
Germanium
Tin
Phosphorus
Antimony
Boron
Fluorescence
Cancer

be relatively easily tuned allows for the introduction of metallocorroles as key components in advanced systems, such as for photovoltaic cells and imaging procedures in living organism.

1. Introduction

Corroles are synthetic tetrapyrrolic macrocycles from the porphyrinoid family, whose best known members are the naturally occurring porphyrins – present in heme enzymes, cytochromes, myo- and hemoglobin (as iron chelates in all these cases) – the di- and tetra-hydro porphyrins in magnesium chelated chlorophyll and bacteriochlorophyll, and the cobalt coordinating ligand corrin present in Vitamin B_{12} [1]. Although the name "corrole" is derived from "corrin" [2], these two macrocycles share only an identical C19 carbon skeleton (rather than C20 in porphyrins and chlorophylls). Corroles are however aromatic (18π electrons conjugation) and carry three NH protons, while corrins are not aromatic and contain only one NH proton (Scheme 1). In fact, corroles are much more closely related to porphyrins than to corrin by virtue of aromaticity, photophysical properties and the coordination chemistry of their metal complexes. The "periodic table" of corrole metal complexes is still not as rich as that of porphyrins, but it is constantly increasing. In this context, it is essential to point out the importance of ionizable NH protons (one in corrin, two in porphyrins, vs. three in corroles) in dictating that coordination compounds with divalent elements (Mg^{II}, Zn^{II}, Fe^{II}, Ni^{II} and many more) are common for porphyrins but rare for corroles. One other very important outcome is that low valent corrole transition metal complexes are much more reactive than their porphyrins analogs. This is most relavent for the activation of small molecules such as O_2 and CO_2 [3,4].

The first corrole was reported in 1964 by Johnson and Kay, who synthesized it as part of their work on synthetic models of Vitamin B_{12} [5]. Nobel laureate Dorothy C. Hodgkin, who focused on X-ray crystallography of Vitamin B_{12}, was also the one who reported the first X-ray structural determination of a free-base (metal free) corrole [6]. Nevertheless, the chemistry of corroles remained largely undeveloped for decades because of severe synthetic obstacles. This may be appreciated by the book chapters that reviewed all the up to 1999 reports about the synthesis of corroles and the coordination chemistry of the corresponding metal complexes [7]. Incidentally, the first one-pot methodologies for facile synthesis of 5,10,15-triarylcorroles (aryl groups on the three *meso*-carbon atoms) (Fig. 1) were disclosed at that same year [8]. The synthetic developments truly reshaped corrole chemistry, as reflected in a very large increase in published papers, the many research groups that became active on various aspects of corroles, and in the elucidation of many novel features [9,10]. These include stabilization of high valent transition metal ions and unique reactivity of low valent metallocorroles, novel photophysical properties, large NH acidity and facile synthetic manipulations. Most importantly, these advances allowed for utilization of corroles and metallocorroles in catalysis, as key component of sensors and solar cells, and as drug candidates in medicine-oriented research [11].

The surprisingly large number of reviews that were published since the introduction of triarylcorroles in 1999 focused on synthetic methodologies, physical properties and special features of the macrocycle and various applications, but not on their coordination chemistry [9]. The corrole chelates that were published until now may be divided into three main groups: (a) early and late transition metals: Ti, V, Ni, Cu, Ag; (b) group 6–9 transition metals: Cr, Mo, Mn, Re, Fe, Ru, Co, Rh, Ir; and (c) main group elements: Zn, Ga, Al, Ge, Sn, Sb, P, B. Interestingly, no lanthanides or actanides were reported yet. The emphasis of this review is on the coordination chemistry of main group complexes of 5,10,15-triarylcorroles. This includes the synthesis of the corresponding complexes, their spectroscopy, electrochemistry, and crystallography, as well as discussions about their chemical reactivity/stability features.

1.1. General features of corrole chelates, shared by transition metals and main group elements

The procedures for metal insertion into **1** and other triarylcorroles are very simple and normally all N-pyrrole atoms participate in metal binding as to provide a *trianionic* equatorial coordination sphere (Scheme 2). Pyridine appears to be the most general solvent, similar to the role of DMF for insertion of metal ions into porphyrins. As for the metal source, metal-chloride and metal-acetate salts are most commonly used. Cases in which not all N atoms participate

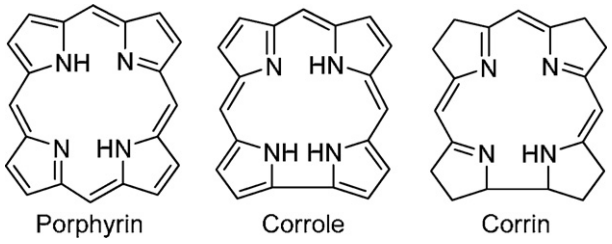

Scheme 1. The basic skeleton of porphyrin, corrin, and corrole.

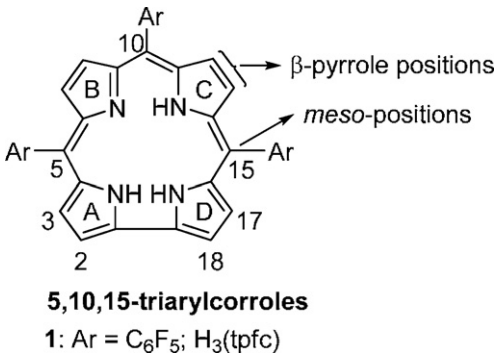

Fig. 1. The general structure of 5,10,15-triarylcorroles such as H_3(tpfc) (Ar = C_6F_5, **1**).

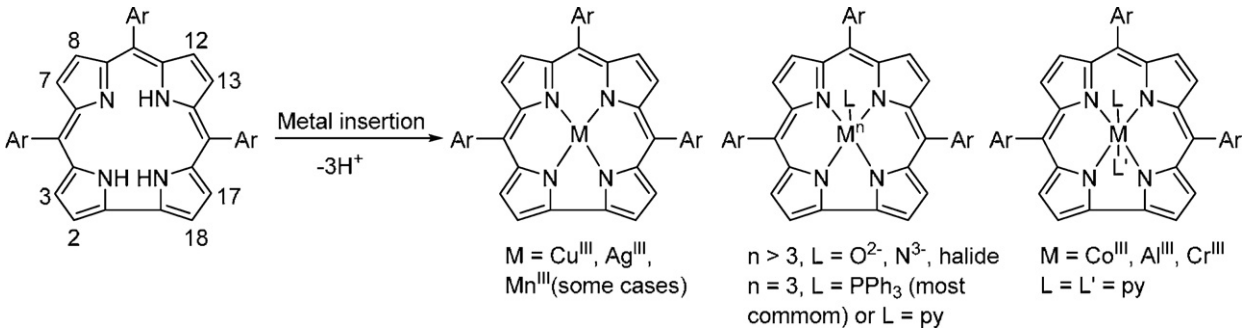

Scheme 2. Transformation of free-base corrole into 4-, 5- and 6-coordinate metallocorroles, with representatives of each case.

in the bonding are quite rare, but exist in the cases of rhodium(I) [12,13], (oxo)vanadium(IV) and (oxo)titanium(IV) corroles [14]. 4-coordinate complexes that contain metal ions in their trivalent state are also rare, with the d^8 copper(III) and silver(III) corroles as the main exceptions [15,16]. The most commonly adopted coordination geometry of corroles is square pyramidal, because out of the N4 plane displacement of the metal ion is beneficial for both the metal and the corrole. The framework of the corrole in these cases is domed and each metal adopts bond lengths that are characteristic of its oxidation state. The affinity of corrole-chelated metal ions for a sixth ligand as to form 6-coordinated complexes is quite low (*vide infra*) and most reported complexes of this kind contain pyridines as axial ligands. All 6-coordinate metallocorroles, including with NMe_3 and fluorides, display a very planar macrocyclic structure [17,18]. Selected X-ray crystallographic structural information is presented in Tables 1 and 2, the latter of which contains all pyridine-coordinated metallocorroles.

2. Zinc(II) corroles

While zinc is formally part of the d-block series of elements, its properties are much more in common with main group elements than with transition metals. In addition, it may safely be stated that zinc(II) porphyrins are the most intensively investigated non-transition metal complexes, regarding both fundamental and applicative science [33], and it is hence relevant to provide information about zinc(II) corroles in this review. From the point of view of photosynthesis and attempts for mimicking the process by synthetic systems, magnesium(II) porphyrins might be even more interesting, but magnesium insertion into porphyrin requires harsh reaction conditions and demetallation is extremely facile. In contrast with the above, neither magnesium(II) nor zinc(II) corroles are known and the reason for that is very simple: corroles act as trianionic rather than dianionic ligands. The validity of the above statement has been proved by the coordination chemistry of N-alkylated corroles (Scheme 3) [24,34].

Table 1
Crystallographic information about various triarylcorrole metal complexes, excluding pyridine-coordinated metallocorroles.[a]

Complex	*L*	*L′*	M-axial ligand bond lengths [Å]	M–N(pyrrole) bond lengths average [Å]	Ref.
Main group elements					
Sb(tpfc)$(F)_2$	F	F	1.940, 1.932	1.975	[18]
Sn(tpfc)Cl	Cl	–	2.330–2.337	2.045	[19]
Ge$(tpc)_2$(O)[b]	O (μ-oxo)	–	1.718–1.773	1.905	[20]
Transition metals					
Cu (tdcc)[b]	–	–	–	1.883, 1.885	[15]
Ag (ttc)	–	–	–	1.954	[16]
Cr(tpfc)(O)[b]	O	–	1.57	1.93	[21]
Mo(tpfc)(O)	O	–	1.684	2.036	[18]
Fe(tpfc)Cl	Cl	–	2.238	1.901	[22]
Fe(tpfc)(NO)[b]	NO	–	1.639, 1.648	1.909	[23]
Fe(tdcc)(NO)	NO	–	1.641	1.910	[23]
Fe$(tpfc)_2$(O)	O (μ-oxo)	–	1.709, 1.726	1.903, 1.908	[24]
$[Ru(tpfc)]_2$	Ru	–	2.182	1.972	[25]
Ru(tpfc)(NO)[b]	NO	–	1.712, 1.718	1.980	[25]
Mn(tpfc)$(OPPh_3)$	$OPPh_3$	–	2.075	1.916	[26]
Mn(tpfc)Br	Br	–	2.428	1.925	[27]
Mn(tpfc)Cl	Cl	–	2.312	1.932	[27]
Mn(IV)(oedpc) I[c]	I	–	2.6626	1.932	[28]
Mn(III)(tpfc)(NAr)	NAr	–	1.613	1.916	[29]
Rh(tpfc)(PPh_3)	PPh_3	–	2.222	1.965	[22]
Rh(tpfc)(PPh_3)(py)[b]	PPh_3	py	M–N: 2.212, 2.241; M–P: 2.297, 2.303	1.959, 1.960	[30]
Rh(tdcc)(PPh_3)(py)	PPh_3	py	M–N: 2.185; M–P: 2.314	1.963	[30]
$_n$Co(tpfc)(PPh_3)	PPh_3	–	2.205	1.879	[31]
Co$(R_2$-tpfc$)(PPh_3)$[d]	PPh_3	–	2.225	1.87	[32]
Ir(tpfc)$(NMe_3)_2$	NMe_3	NMe_3	2.185	1.965	[17]

[a] For information about 5- and 6-coordinate complexes with pyridine as the axial ligand(s) see Table 2.
[b] There are two crystallographically independent corrole species in the asymmetric unit of these structures.
[c] Not a triarylcorrole.
[d] Contains a tpfc ligand with two sulfonamide head groups on C2 and C17.

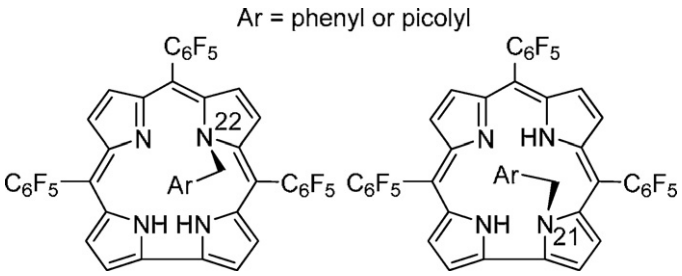

Scheme 3. The structures of chiral N^{21}- and the N^{22}-substituted corroles (only one of the two enantiomers is shown for each case), obtained from corrole **1**.

Single N-alkylation of corroles leads to diprotonic products, into which zinc(II) may be inserted as easy as into regular porphyrins [35]. The diamagnetic derivatives that have been obtained from the reaction with zinc acetate in pyridine were analyzed by NMR; and two such complexes have been further characterized by X-ray crystallography. There are several interesting aspects that have been revealed from these investigations. All complexes are 5-coordinate, by four N atoms from the macrocyclic ligand and one pyridine molecule. The latter is provided either externally or internally from the N-pycolyl substituent, as shown for the Zn^{II}(N^{21}-picolyl-tpfc) complex (Scheme 4).

Interestingly, the external pyridine is almost certainly bound to the same site as the internal picolyl, as indicated by the large downfield shift ($\Delta\delta$ = 2.33 ppm) of the benzylic protons upon coordination (a similar experiment with the zinc(II) complex of N^{21}-benzyl-tpfc revealed that the benzylic protons are essentially not affected). The pyridine moiety of the picolyl substituent which is attracted as the axial ligand can be easily seen in the structure of the complex (Scheme 4b). The strong coordination is reflected in Zn–N bond lengths of 2.073–2.093 Å (for two crystallographically independent enantiomers). The zinc(II) ion is located 0.42 Å above the mean plane of the four nitrogen atoms and adopts a slight distorted square–pyramidal geometry. Such a combination of a Lewis acidic metal and the nucleophilic pyridine in a chiral environment creates an excellent reaction center. The most unique aspect is that all these complexes are chiral, because corroles (but not porphyrins) lose all their symmetry elements upon N-alkylation. This has been demonstrated via separation of these C_1 complexes by the aid of HPLC on a chiral stationary phase and the circular dichroism (CD) spectra of the resolved enantiomers. A major advantage of these chiral corroles is their very easy two-step preparation, in contrast to the preparation of chiral porphyrins and salens that consists of many synthetic steps and relies on the covalent attachment of molecules from the "chiral pool".

3. Gallium(III) corroles

Based on density functional theory (DFT) calculations, Ghosh and Jynge proposed that gallium(III) may fit perfectly into the coordination core of corroles [36], thus providing the opportunity of obtaining a reference complex for transition metal corroles. This hypothesis was later proved correct indeed by Bendix et al: the metallation of **1** (Fig. 1) and of 5,10,15-tris(heptafluoropropyl)corrole [H_3(thfpc)] by $GaCl_3$ in pyridine was facile and proceeded with essentially quantitative yields (Scheme 5) [37].

One advantage of the non-transition metal complexes is that one can easily study important aspects of the corrole macrocycle, such as the electron density at the various positions, the energy gap between the highest occupied and lowest unoccupied molecular orbitals (the HOMO–LUMO gap), and the characteristics of the π-cation radicals obtained upon oxidation of the corrole. The publication of Bendix et al. describes the X-ray structure of the Ga(tpfc)(py) complex, its electronic spectrum and the large changes upon corrole-oxidation, the ESR spectrum of the oxidized complex, and DFT calculations on both the neutral and the one-electron oxidized product [38].

Recrystallization from benzene/heptane solutions (with a few drops of pyridine) afforded X-ray quality crystals of the pyridine-coordinated gallium(III) complexes, Ga(tpfc)(py) and Ga(thfpc)(py)

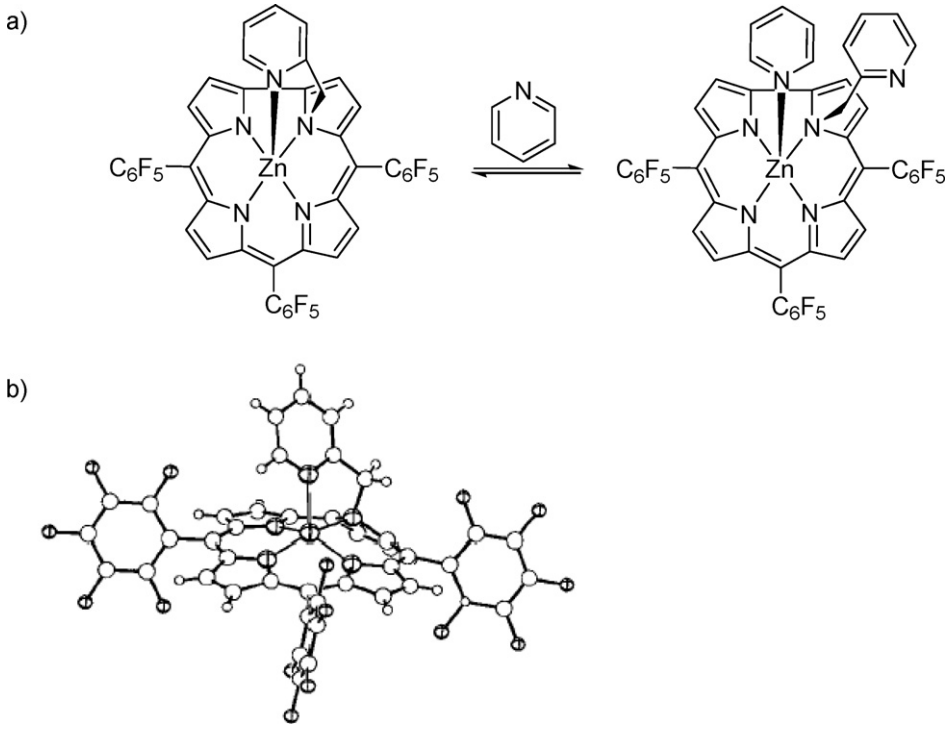

Scheme 4. (a) Addition of pyridine to Zn^{II}(N^{21}-picolyl-tpfc) and (b) one of the crystallographically independent enantiomers contained in the crystals of Zn^{II}(N^{21}-picolyl-tpfc). Figure was reproduced from Ref. [35b], with permission of the copyright holders.

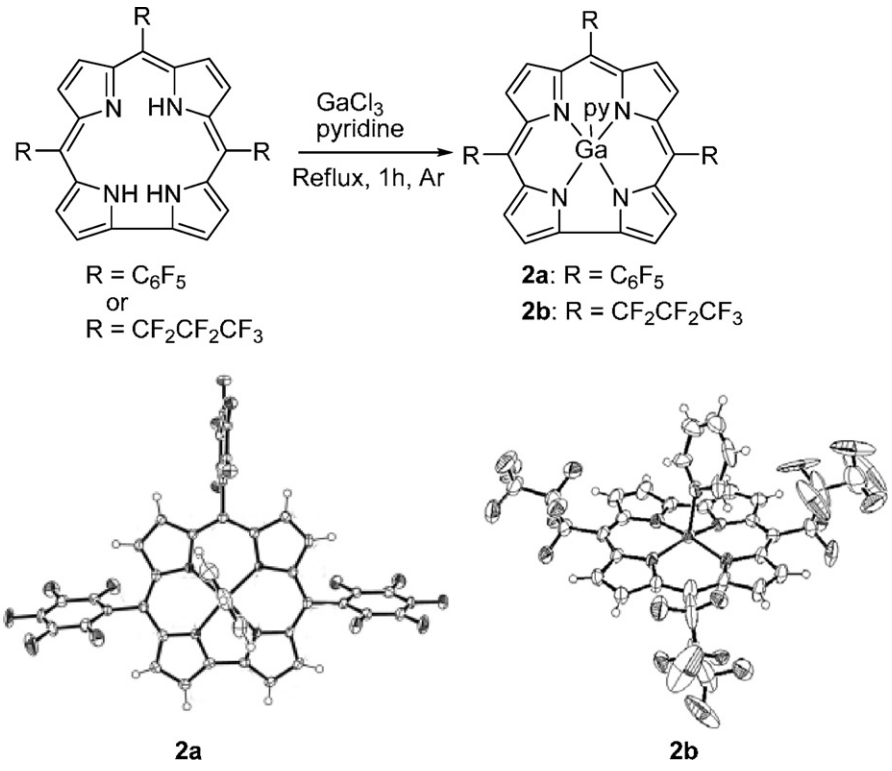

Scheme 5. Synthesis of *meso*-substituted-corrolato gallium(III) and the molecular structures of these 5-coordinated complexes. Figures were reproduced from Refs. [37,38], with permission of the copyright holders.

(Scheme 5) [37,38]. The motivation in the synthesis of Ga(thfpc)(py) was the potential utilization in bioinorganic chemistry, because its flexible *meso*-C_3F_7-substituents are advantageous for replacing protoporphyrin IX in hemo-proteins. The flexibility of the *meso*-substituents may be appreciated by comparing the X-ray structures of the free-base ($R = CF_2CF_2CF_3$) and the gallium corrole, Ga(thfpc)(py) (**2b**). The mutual orientations of the C_3F_7 substituents in the free-base and **2b** are different, up–down–down and up–down–up, respectively. The structure of this complex is shown in Scheme 5, which also illustrates the main structural changes that occur upon metallation of H_3(thfpc). Evidently, replacement of the NH protons by the gallium(III) cation, releases to a considerable extent the conformational strain imposed by the former and flattens the corrole ring. Correspondingly, the mean deviations of the outer C–C bonds of the pyrroles with respect to the plane of the four pyrrole nitrogen atoms are much smaller in the gallium(III) complex (varying from −0.25 to +0.25 Å) than in the free-base corrole (from −0.69 to +0.67 Å). A comparison with the structure of Ga(tpfc)(py) (**2a**) revealed that both complexes are 5-coordinated, with one pyridine occupying the axial position and pulling the metal out of the corrole plane: by 0.41 Å in Ga(tpfc)(py) (**2a**) and 0.31 Å in Ga(thfpc)(py) (**2b**). The coordinated pyridine in Ga(tpfc)(py) is also evident in the NMR spectrum by virtue of its upfield shifted resonances: 6.62, 5.77, and 2.44 ppm for H_p, H_m, and H_o, respectively, due to the diamagnetic current effect of the corrole. Changes in the electronic spectrum upon addition of excess pyridine were analyzed in terms of the formation of a hexa-coordinated complex. The binding of pyridine to the metal is strong enough for the high-shifted resonances to be observed by ^{1}H NMR, but also weak enough (reversible) for the ligand to be displaced by pyridine-d_5. A 6-coordinate bis(pyridine)gallium(III) complex was indeed isolated for the 3,17-dinitro-substituted corrole (Fig. 2) [39]. This coordination number is apparently unique to trianionic corroles, as there is no such precedence in gallium(III) complexes of dianionic porphyrins or phthalocyanines.

The gallium(III) corrole **2a** was functionalized to yield a variety of β-pyrrole substituted corroles (Scheme 6). Addition of bromine to a benzene solution of **2a** resulted in the fully brominated gallium(III) corrole Ga(tpfc-Br_8)(py) **3** [40]. By adding the Vilsmeier reagent ($POCl_3$ in DMF) to CH_2Cl_2 solution of **2a**, two formylated gallium complexes were obtained (**4a**, **4b**) [39]. The relative ratio of the products was controlled by varying the amounts of $POCl_3$. Reaction of **4b** with malononitrile resulted in **5**, whose Q-bands are near 700 nm. The two formylated complexes could be excellent precursors of the carboxylated complexes **6a** and **6b**, but the attempts to apply standard procedures for oxidation of aldehydes to carboxylic acids failed. Thus, an alternative route was applied: **6a** and **6b** were synthesized by adding a 20% solution of phosgene in toluene to solution of **2a** and pyridine in toluene. The major product of this reaction was **6a** (58% isolated yield) [12]. Reactions of **2a** with sodium nitrite and tris(4-bromophenyl)aminium hexachloroantimonate (as oxidant) in acetonitrile under argon produced the nitro-substituted gallium corroles **7a**, **7b** and **7c** [39]. By varying the amount of oxidant used between 0.75 and 3.0 equivalents, three products were formed in varying ratios. When less oxidant

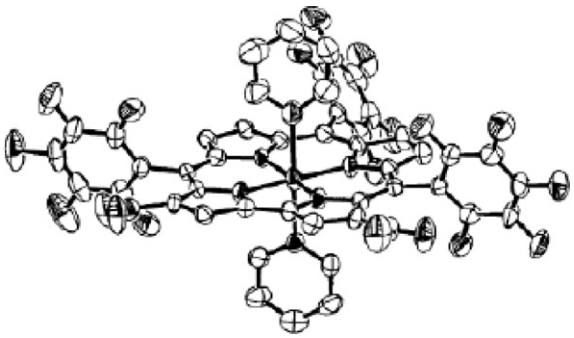

Fig. 2. The X-ray crystal structure of 3,17-$(NO_2)_2$-Ga(tpfc)$(py)_2$, **7b**. Figure was reproduced from Ref. [39b], with permission of the copyright holders.

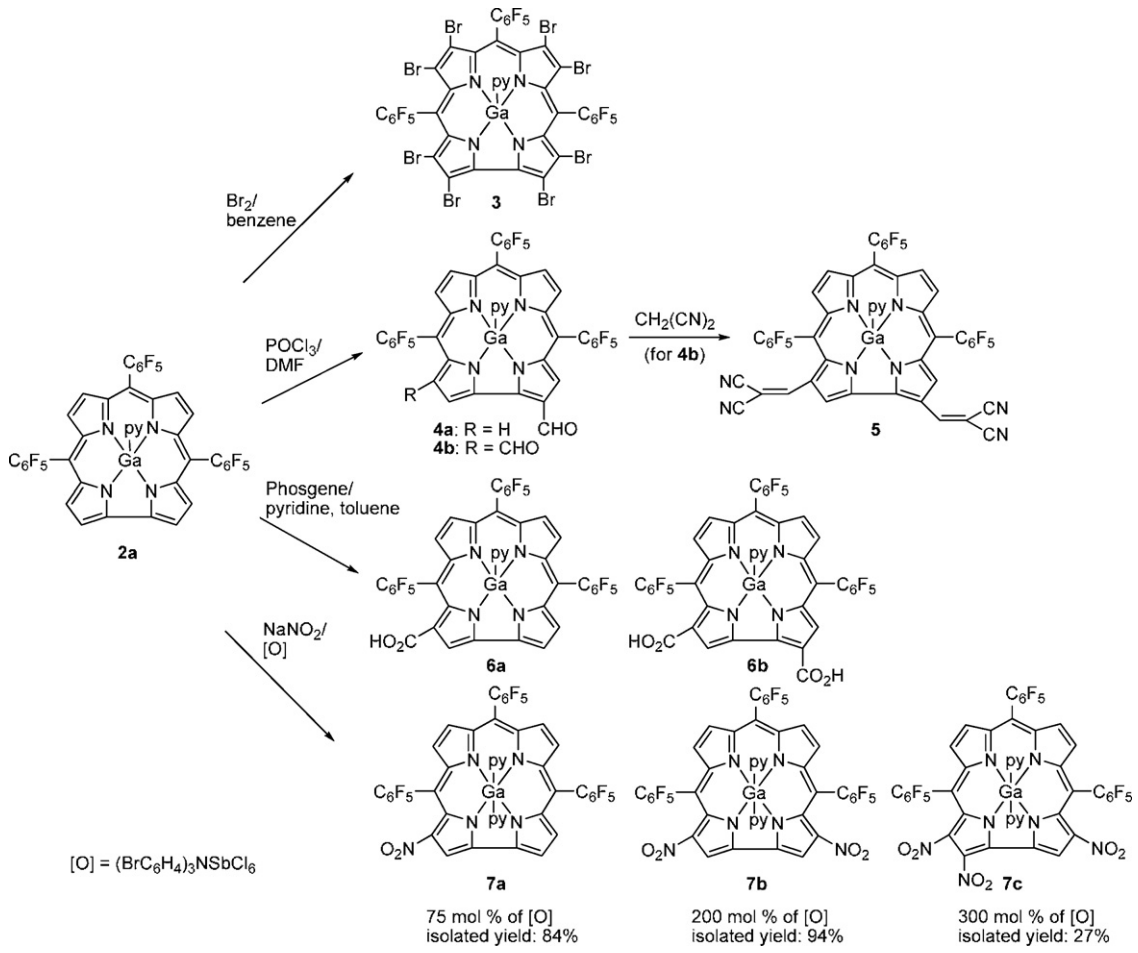

Scheme 6. Synthesis of corrole-functionalized gallium(III) complexes.

was used (75 mol %), the major product was the mono-substituted **7a**. Using more oxidant, greater amounts of the disubstituted **7b** (200 mol%) and the trisubstituted **7c** (300 mol%) were produced. Most importantly, all three products were obtained as single isomers despite of the many other possibilities.

X-ray quality crystals have been obtained for all the nitro-substituted gallium(III) corroles. **7a** and **7c** crystallized as mono-pyridine complexes, although they were observed as bis-pyridine adducts by NMR spectroscopy. In the structure of the 6-coordinate **7b**, the corrole ring is essentially planar with an octahedral coordination environment around the metal. The two pyridine ligands are roughly parallel to each other, with an approximately 14° twist angle between their planes (Fig. 2).

Selected structural parameters of all reported gallium(III) complexes (5- and 6-coordinated) are listed in Table 2, together with data about 6-coordinate aluminum(III), iron(III), cobalt(III), chromium(III), rhodium(III) and iridium(III) complexes. The X-ray structure of the 5-coordinate Ga(tpfc)(py) (entry 1) shows that the geometry of the metal is square pyramidal with the gallium(III) center displaced 0.41 Å out of the N4 plane, and that the corrole is slightly domed (all four pyrrole rings are planar and point toward the metal). The Ga–N_{py} bond is much longer (2.033 Å) than the Ga–$N_{pyrrole}$ bonds (average 1.94 Å), but, nevertheless, quite short for a gallium–pyridine bond (compare e.g. 2.121–2.151 Å in $[Ga(N_3)_3(py)_3]$). The same holds for Ga(thfpc)(py) and for the carboxyl- and nitro-substituted gallium complexes

Table 2
Selected structural parameters in Ga(cor)$(py)_n$ (n = 1 or 2), and of the bis-pyridine M(III) analogs (M = Al, Fe, Co, Cr, Rh, Ir).

Entry	Complex	M deviation [Å] from the N_4(corrole) plane	M–pyridine bond lengths [Å]	M–N(pyrrole) bond lengths range [Å]	Axial-py twist angle (°)	Ref.
1	Ga(tpfc)(py), **2a**	0.41	2.033	1.936–1.944	–	[38]
2	Ga(thfpc)(py), **2b**	0.31	2.073	1.923–1.945	–	[37]
3	3-(CO_2H)-Ga(tpfc)(py), **6a**	0.40	2.024	1.933–1.970	–	[12]
4	3-(NO_2)-Ga(tpfc)(py), **7a**	0.376	2.039	1.926–1.972	–	[39]
5	2,3,17-$(NO_2)_3$-Ga(tpfc)(py), **7c**	0.301	2.055	1.909–1.958	–	[39]
6	3,17-$(NO_2)_2$-Ga(tpfc)$(py)_2$, **7b**	0.053	2.234, 2.284	1.909–1.940	14	[39]
7	Al(tpfc)$(py)_2$, **8**	0.003	2.215, 2.201	1.887–1.899	3.6	[43]
8	Fe(tpfc)$(py)_2$	0.001	2.028, 2.032	1.865–1.923	8.8	[24]
9	Co(tpfc)$(py)_2$	0.002	1.994, 1.994	1.873–1.900	2.3	[42]
10	Cr(tpfc)$(py)_2$	0.002	2.109, 2.129	1.926–1.952	10.8	[44]
11	Rh(tpfc)$(py)_2$	0.015, 0.009	2.060, 2.071	1.938–1.976	4.2, 2.4	[13]
12	Ir(tpfc)$(py)_2$	0.005	2.052, 2.066	1.947–1.979	7.0	[45]

(entries 2–5), in which the gallium(III) ion deviates by 0.4 Å (in the carboxyl derivative), 0.376 Å (in the mononitro derivative), and 0.301 Å (in the trinitro-substituted corrole) from the plane of the four pyrrole nitrogen atoms. On the other hand, the dinitro-substituted complex is 6-coordinate with two axial pyridine ligands bound to the gallium(III) ion from opposite sides at a slightly longer coordination distance (2.234, 2.284 Å) than in the 5-coordinate complexes (2.033–2.073 Å) (entry 6). The features of the 6-coordinate bis-pyridine complex are quite different from that of the earlier discussed 5-coordinate corroles; the corrole is flat with an octahedral coordination environment around the metal and an almost perfect mutual linear alignment of the coordinated pyridines. These features are very similar to those found in crystal structures of related bis-pyridine complexes of aluminum(III), iron(III), cobalt(III) and chromium(III), rhodium(III) and iridium(III) (entries 7–12). Chromium(III) has a somewhat larger radius than iron and cobalt, yet it is still located perfectly in the plane defined by the four inner nitrogen atoms. This is accompanied, however, by a systematic increase in Cr–N compared to M–N distances in related complexes. The data collected in Table 2 reveal that in all reported bis-pyridine metallocorrole complexes the two pyridine molecules are nearly parallel to each other with a twist angle that ranges between 2.3° and 14° (entries 6–10). This is in contrast with iron(III) porphyrins whose axial ligands adopt perpendicular orientation as well in certain cases [41]. An interesting aspect is that comparison of the bis-pyridine complexes of the non-transition metal complexes (Al^{III} and Ga^{III}) with the transition-metal analogs (Cr^{III}, Fe^{III}, Co^{III}, Rh^{III}, Ir^{III}) reveals that the metal N-pyridine bond lengths are considerably longer in the former than in the latter cases (2.2–2.28 Å vs. 1.99–2.13 Å). This phenomenon reflects metal–ligand π bonding interactions, apparently increasing in importance for $Co^{III} > Fe^{III} > Cr^{III}$ and $Ir^{III} > Rh^{III}$. For the non-transition metal complexes it provides a clue about the Lewis acidity of the central atom ($Al^{III} > Ga^{III}$, according to the shorter bonds to pyridine in the former case), which is consistent with recently reported equilibrium constants (*vide infra*) indeed. Extreme differences (but not small ones) between bond lengths in transition and non-transition bis-pyridine coordinated metallocorroles may also be interpreted similarly. For example, the bis- to mono-pyridine dissociation constants of gallium(III) and cobalt(III) are 1 and 3.3×10^{-5} M, respectively [42], which is reflected in very large differences in Ga–N(pyridine) and Co–N(pyridine) bond lengths (2.234–2.284 and 1.994, respectively).

The redox potentials of main group corrole chelates and the spectroscopic features of the one election oxidized complexes provide very useful information, since these necessarily contain a corrole π-radical. On the other hand, in corrole transition metal complexes it is much harder to distinguish between metal- and corrole-centered redox processes because of strong coupling of π and d electrons [46]. The cyclic voltammogram (CV) of Ga(tpfc)(py) (**2a**) shows a reversible oxidation wave with $E_{1/2}$ = 0.75 V vs. SCE. This value is much lower than the corresponding values of 1.13 and 1.20 V of the related 5-coordinate complexes, Ge(tpfc)(OH) and Sn(tpfc)(Cl), respectively. This is reminiscent of similar observations in metalloporphyrins, in which the redox potential of the macrocycle correlates with the electronegativity of the metal ($Ge^{IV} \geq Sn^{IV} > Ga^{III} > Zn^{II} > Mg^{II}$) [47]. The oxidation potential of Ga(tpfc)(py) suggests that it can be chemically oxidized to the corresponding corrole π-cation radical complex, $[Ga(tpfc^{\bullet})(py)]^+$, by the commercially available compound tris(4-bromophenyl)aminium hexachloroantimonate ($E_{1/2}$ = 1.11 V). This was the case indeed: Fig. 3 shows the UV/vis spectra of Ga(tpfc)(py) and $[Ga(tpfc^{\bullet})(py)]^+$, as well as the EPR spectrum of the latter.

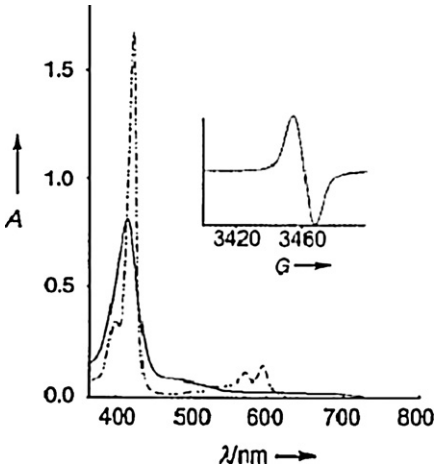

Fig. 3. UV/vis spectra of Ga(tpfc)(py) (broken line) and $[Ga(tpfc^{\bullet})(py)]^+$ (full line), and the EPR spectrum of $[Ga(tpfc^{\bullet})(py)]^+$ (inset), all in CH_2Cl_2 at room temperature.

The electronic spectrum of Ga(tpfc)(py) is dominated by an intense and quite narrow Soret band at 398–412 nm and much weaker Q-bands. Upon one-electron oxidation to the corrole π-cation radical complex, the Soret band shifts to the blue and loses more than half of its intensity. This phenomenon is very similar to what is considered as one of the characteristics of porphyrin π-cation radicals. The other prominent feature of porphyrin π-radical complexes is the appearance of new bands in the >600 nm region. This is hardly seen for $[Ga(tpfc)(py)]^{+\bullet}$, which suggests that it is of limited utility in distinguishing between corrole- and metal-based oxidation in transition metal corroles. The EPR spectrum of the corrole π-cation radical complex also displays only a singlet, which is another difference relative to the very rich spectra of tetraarylporphyrin π-radical derivatives [48]. DFT calculations, performed for both Ga(tpfc) and $[Ga(tpfc)]^{+\bullet}$, provided a rational. They disclosed two very closely spaced highest occupied molecular orbitals, depicted in Fig. 4 for Ga(tpfc), that resemble the a_{1u} and a_{2u} orbitals of porphyrins. The spin density on the nitrogen atoms for both possible electronic configurations of $[Ga(tpfc)]^{+\bullet}$ was, however, found to be much smaller than in analogous porphyrin radical complexes. This readily explains why the corresponding EPR coupling constants could not be observed experimentally.

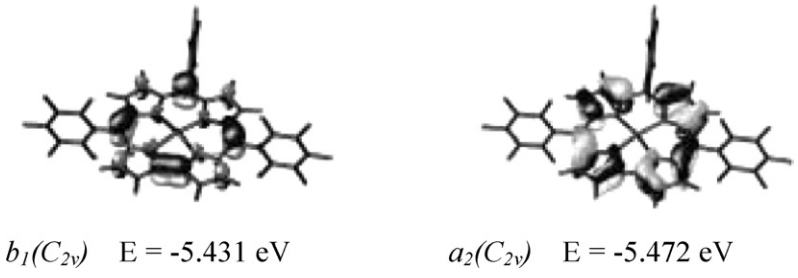

Fig. 4. Perspective drawing of the calculated electron densities of the two highest occupied molecular orbitals of Ga(tpfc).

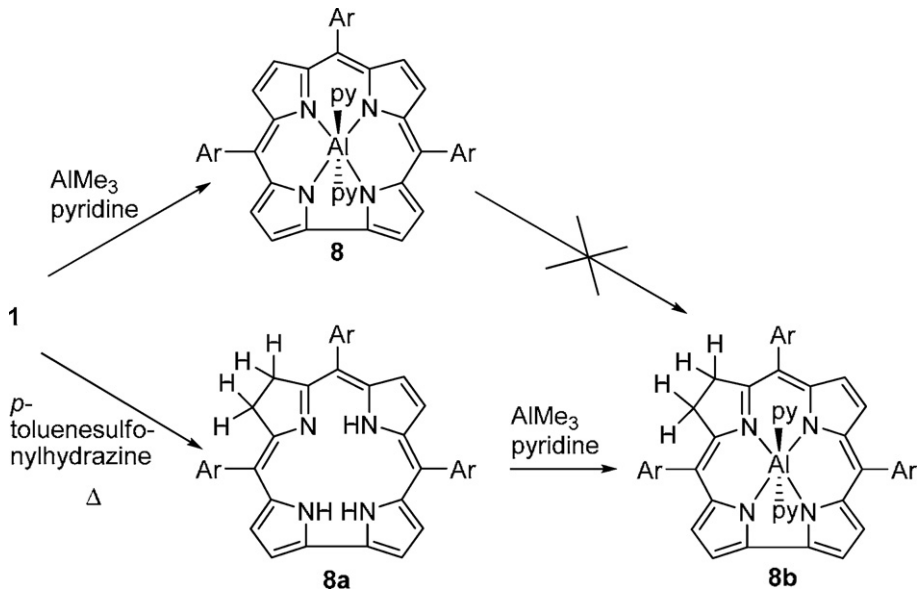

Scheme 7. Synthesis of aluminum(III) corrole (8), corrolin (**8a**), and aluminum(III) corrolin (**8b**).

Since the redox processes of the non-transition metal corroles necessarily involve only the macrocycle, the difference between the half wave potentials for one-electron oxidation and reduction was used for determining the *electrochemical* HOMO–LUMO gap (considered as correlated, but not necessarily identical to the Frank Condon like difference between MO levels). A value of 2.20 ± 0.15 V was obtained by utilizing a series of non-redox-active metal complexes of **1**, which is very similar to those of metal complexes of porphyrins and octaethylcorrole [47,49]. This information is of prime importance, as it provides an independent clue for distinguishing between metal- and corrole-centered redox processes in transition metal complexes.

Another interesting phenomenon is that metallation of H_3(tpfc) by gallium(III) resulted in a very strong increase in fluorescence intensity, which contrasts sharply with the decrease in fluorescence intensity upon zinc(II) insertion into porphyrins. This phenomenon is intimately related to the earlier discussed large effects of metallation on the structural aspects of corroles, as discussed later in the more detailed account of the photophysical properties of main group corroles.

4. Aluminum(III) corroles

The difference between the diprotonic porphyrins and triprotonic corrole dictates that aluminum(III) corroles may be regarded as analogs of magnesium(II) porphyrins. The first aluminum(III) corrole was reported in 2002: hexacoordinated Al(tpfc)(py)$_2$ (**8**) was obtained in quantitative yield from the reaction of **1** with Me_3Al in pyridine (Scheme 7) [50]. The ^{1}H NMR spectrum of the complex displayed four different β-pyrrole CH resonances (2H each, consistent with C_{2v}-symmetry), of which the two with $J = 4.6$ Hz were confidently assigned to pyrroles B and C by analogy to porphyrins and those with $J = 4.0$ Hz to pyrroles A and D by analogy to 2,2′-bipyrroles. Modern NMR techniques confirmed these assignments [51]. Two coordinated pyridine molecules per metal were also observed in the ^{1}H NMR spectrum, implying that the complex remains 6-coordinate even in solution.

Because of its extremely intense fluorescence (*vide infra*), it was of interest to examine if a corrole-based chlorophyll analog may be prepared. Attempts for direct hydrogenation of the macrocyle of **8** did not succeed, but this task was achieved on the free-base corrole **1**. Metal insertion into the thus obtained 7,8-dihydrocorrole (**8a**, termed corrolin), allowed for the isolation of the aluminum(III) complex **8b**, which displayed the spectroscopic features expected from a chlorophyll analog indeed. What is more, the fluorescence quantum yield of the aluminum(III) corrolin **8b** ($\phi_f = 0.62$) is almost twice as large as that of the natural pigment, chlorophyll-a ($\phi_f = 0.32$) [50].

The crystal structure of the bis-pyridine aluminum(III) corrole **8** reveals that the metal ion is located in the plane of the corrole macrocycle and that the two axial pyridine molecules are nearly parallel to each other with a twist angle of 3.6° [43]. Close inspection of the two pyridine molecules suggests that they bend slightly toward each other with a bending angle of 171.5°. The interatomic distances between the Al(III) center and the surrounding N atoms in both equatorial and axial positions are within the expected range of Al–N bond distances: about 1.9 and 2.2 Å, respectively.

The equilibrium constant between 5-coordinate Al(tpfc)(py) and 6-coordinate Al(tpfc)(py)$_2$ was determined in a later publication [52]. The two order of magnitude larger equilibrium constant relative to the same corrole, but with gallium(III) rather than aluminum(III), shows that the Lewis acidity of the latter is much more significant than that of the former.

5. Germanium, tin, and phosphorus corroles

Germanium(IV), tin(IV), and phosphorus(V) complexes were prepared in high yields by heating corrole **1**, dissolved in either pyridine or DMF, with excess $GeCl_4$, $SnCl_4$, and $POCl_3$, respectively [24]. In all cases, the crude reaction mixture consisted of the desired metallation product, but as mixtures of chloro- and hydroxo-coordinated complexes (observed by NMR). Pure Sn(tpfc)Cl was obtained by extensive washing with concentrated HCl solutions, while treating the germanium(IV) and phosphorus(V) complexes by flash chromatography on wet silica resulted in the hydroxo-coordinated products, Ge(tpfc)OH and P(tpfc)(OH)$_2$. In contrast to the hydrolytic lability of the chlorides, the coordinated hydroxide is substitution-inert, as indicated by the lack of conversion into the chloro-coordinated complexes via treatment with concentrated HCl solutions. The hydroxo protons and couplings between P and the β-pyrrole-H-protons are apparent in the NMR spectra of P(tpfc)(OH)$_2$ at the high-field (−5.3 ppm, broad singlet) and low-field parts (8.6–8.9 ppm, double doublets), respectively. The electronic spectra of all three complexes are very similar, with

Table 3
Half wave potentials (in V vs. sce, in CH_2Cl_2) for oxidation and reduction of corrole metal complexes.

Complex	Cor^+/Cor	Cor/Cor^-	ΔE [V][a]	M^n/M^{n-1}	Ref.
Sn(oec)Ph	0.47	−1.74	2.21		[53]
Sn(oec)Cl	0.67			−1.46[b]	[53]
Sn(tpfc)Cl	1.20	−0.94	2.14		[24]
Ge(tpfc)OH	1.13	−0.99	2.13		[24]
P(tpfc)$(OH)_2$	1.05	−1.05	2.10		[24]
Ga(tpfc)(py)	0.75				[38]
Ga(bstpfc)(py)	≥0.7[c]				[54]
Al(bstpfc)(py)	0.52[c]				[54]

[a] The difference in potentials for the first oxidation and the first redox potential of the corrole.
[b] Sn^{IV}/Sn^{II}.
[c] bstpfc = 2,17-bis-sulfonato-5,10,15-(tpfc), in CH_3CN.

a sharp Soret band at 410–416 nm and two main Q-bands at 550–600 nm. Electrochemical investigations for these complexes (Table 3) revealed a 0.53 V increase in the oxidation potential on moving from the electron-rich corrole complex Sn(oec)Cl to the analogous Sn(tpfc)Cl, with an electron-poor corrole. The constant difference of 2.12 ± 0.02 V between the oxidation and reduction potentials of Sn(tpfc)Cl, Ge(tpfc)OH, and P(tpfc)$(OH)_2$, clearly proves that in all cases only the corrole is involved in the redox processes. This is different from Sn(oec)Cl, in which the metal is reduced at −1.46 V, much before the reduction of that electron-rich corrole is expected (a value of −1.96 V was calculated). The HOMO–LUMO gap of these tpfc complexes is similar to the 2.12 ± 0.02 V value previously mentioned for gallium(III) complex of the same corrole and of many oec complexes [49]. In fact, both are in the range of 2.20 ± 0.15 V reported for a large variety of metalloporphyrins [47]. The important outcome of these investigations is that if a metallocorrole displays two redox potentials that are separated by significantly less than 2.0 V, at least one of them is most likely to be metal-centered. The effect of the chelated metal ion is also very large, as may be appreciated by the Cor/Cor^+ redox potential changing from 1.2 for $[Sn(Cl)]^{3+}$ to 0.52 for $[Al]^{3+}$.

The results of the EPR examination of the corrole radical complexes were also reported, with special attention to identify possible hyperfine splitting due to considerable spin density on either the nitrogen atoms or on the metal (for Ge and P) in the one-electron oxidized complexes. However, only unresolved spectroscopic lines were obtained, with linewidths (halfwidth at halfheight) of 4, 20, and 6 G for Sn(tpfc)Cl, Ge(tpfc)OH, and P(tpfc)$(OH)_2$, respectively. This suggests that the majority of the spin density is concentrated on the quaternary α-pyrrole carbons, similar to porphyrin radicals with an A_{1u} ground state. This conclusion is consistent with the earlier discussed DFT calculations on Ga(tpfc), which disclosed that the spin density on the nitrogen atoms in the a_{1u}-like and a_{2u}-like orbitals is significantly lower than in analogous porphyrins. One outcome from these investigations is that the spectroscopic properties of corrole radicals are significantly less distinctive than that of porphyrin radicals. However, the constant difference between the first oxidation and reduction potentials of corroles remains a very useful tool for distinguishing between metal and corrole centered oxidation [55].

Paolesse and co-workers reported the preparation of germanium(IV) complexes of triphenylcorrole (tpc) from the reaction of H_3(tpc) with $GeCl_4$ in DMF [20]: a μ-oxo dimer Ge(tpc)$_2$(O) and the methoxy-coordinated mononuclear complex Ge(tpc)(OMe). The X-ray structure of the μ-oxo dimer reveals a square–pyramidal coordination sphere for the germanium(IV) ion, lying 0.439 Å above the N_4 corrole plane, and that the N_4 planes within each dimer are not parallel, forming dihedral angles of 19.4(6)° and 19.9(5)° (Fig. 5a).

Treatment of either the methoxy or the μ-oxo dimer with HCl resulted in the chlorogermanium(IV) complex, Ge(tpc)Cl. Reaction of Ge(tpc)(OMe) with Br_2 in $CHCl_3$/Py afforded the partially brominated hexabromo derivative, possessing six bromine atoms on the peripheral positions (2,3,8,12,17,18-hexabromo-Ge(tpc)(OMe), Fig. 5b). This confirms the higher reactivity of the pyrrolic positions on the two directly linked pyrroles A and D and provides an indication of the substitution regioselectivity on pyrrole subunits B and C (see Fig. 1). The reaction leads to the substitution of the protons H8 and H12, while H7 and H13 remain unreacted, and thus only one of the three possible regioisomers is obtained. This result confirms the previously reported selectivity by Gross and Mahammed, where deuteration of tris(pentafluorophenyl)corrole

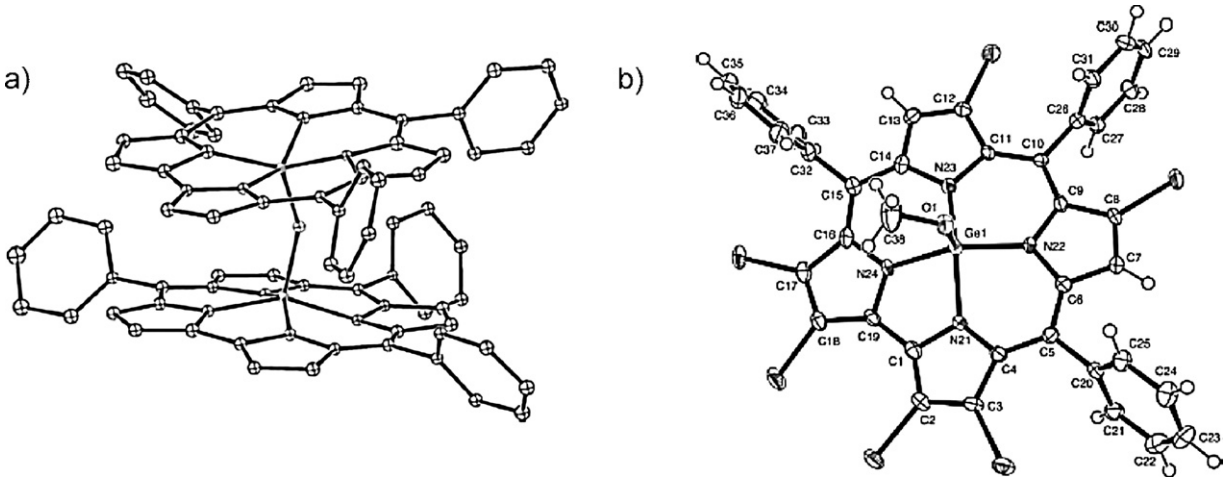

Fig. 5. (a) X-ray structure of one of the two germanium(IV) μ-oxo dimers in the asymmetric unit. (b) 2,3,8,12,17,18-Hexabromo-Ge(tpc)(OMe). Figure was reproduced from Ref. [20], with permission of the copyright holders.

proceeded with a similar reactivity order regarding electrophilic substitution: C3,C17 > C2,C18 ≫ C8,C12 > C7,C13 [56].

The absorption spectra of Ge(tpc)(OMe) and Ge(tpc)Cl are very similar to the one described previously for Ge(tpfc)Cl, while all the bands in the hexabromo derivative are red-shifted similar to the effect of (octa)bromination of gallium(III) corroles. This study also revealed fluorescence and phosphorescence of the derivatives, which are discussed in a separate section. The same research group also reported that the reaction between Ge(IV) triphenylcorroles with Li/Na nitrates/Ac_2O/AcOH leads to the corresponding β-nitro substituted complexes [57]. Only 3-nitro and 3,17-dinitro derivatives, as mixtures of interconvertable mono- and binuclear (μ-oxo) complexes, were obtained by controlling the reaction conditions. The selectivity of nitration is identical to that previously obtained for the gallium(III) complex of tris(pentafluorophenyl)corrole, where the 3-nitro, 3,17-dinitro, and 2,3,17-trinitro derivatives were obtained as single isomers by controlling the amount of oxidant added (**7a**, **7b**, **7c**, Scheme 6). Since the nitro groups affect reduction more than oxidation, the HOMO–LUMO gap is below that of other corroles: 1.90 and 1.76 V for the mono- and bis-substituted cases, respectively. The interactions between the corrole subunits in the μ-oxo dimer may be sensed by electrochemistry, which can be evaluated from the potential difference between the two one-electron oxidation processes.

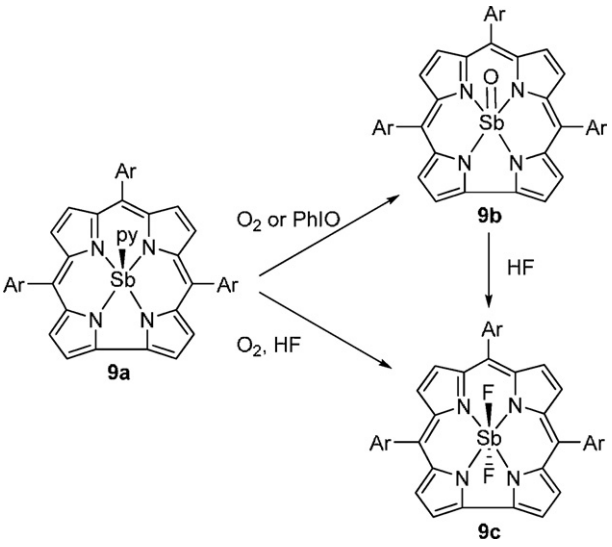

Scheme 8. Synthesis of antimony(III) and antimony(V) corroles.

6. Antimony corroles

The coordination chemistry of antimony corroles is surprisingly rich, as this element may be stabilized in different formal oxidation states and various structural environments. In addition, they have rich redox chemistry and interesting catalytic properties. The isolated complexes consist of 5-coordinate Sb(tpfc)(py) and Sb(tpfc)(O) and 6-coordinate Sb(tpfc)$(F)_2$ (**9a**–**9c**, Scheme 8) [18]. The reaction of **1** with $SbCl_3$ in pyridine afforded Sb(tpfc)(py) in 95% yield: both its ^1H and ^{19}F NMR spectra are consistent with the dominant species in solution to be 5-coordinate, i.e., an antimony(III) corrole with only one pyridine ligated to the axial position. The (oxo)antimony(V) corrole was obtained in quantitative yields from the oxidation of Sb(tpfc)(py), achieved by either O_2 (slow) or PhIO (fast). Treatment of Sb(tpfc)(O) with aqueous HF (48%) led to the *trans*-difluoroantimony(V) complex in 97% isolated yield. Interestingly, the same complex could be prepared directly by treating the antimony(III) corrole with HF under air, via an oxygenation/fluorination pathway.

X-ray crystallography data were obtained for the 6-coordinate complex, Sb(tpfc)$(F)_2$, revealing a very flat structure with short Sb–F bonds and long Sb–N(pyrrole) distances. The Sb(V) ion lies in the center of the N4 core and is coplanar with the pyrrole N-atoms. The deviations of the individual carbon atoms from the mean plane of the 19-membered C framework are within −0.09 to +0.06 Å, with an rms deviation of only 0.04 Å (Fig. 6).

The electrochemical oxidation potentials of the two antimony(V) complexes, Sb(tpfc)(O) and Sb(tpfc)$(F)_2$, necessarily reflect oxidation of the corrole. From the vast differences between the $E_{1/2}$ values (1.10 and 1.47 V for Sb(tpfc)(O) and Sb(tpfc)$(F)_2$, respectively) it is evident that the $[Sb(F)_2]^{3+}$ moiety is much more electron withdrawing than $[Sb(O)]^{3+}$. This effect is less dominant in the reduction process, for which smaller differences ($E_{1/2} = -0.77$ and −0.64 V for Sb(tpfc)(O) and Sb(tpfc)$(F)_2$, respectively) were obtained. The antimony(III) corrole, Sb(tpfc)(py), displayed two redox potentials, of which the one with $E_{1/2} = -1.1$ V corresponds to reduction of the corrole. The other process, at $E_{1/2} = 1.0$ V, is ambiguous and may reflect either oxidation of the corrole or an antimony(III)/antimony(IV) process. While the 2.1 V difference between the two redox couples is consistent with both processes being corrole-centered, as it fits perfectly within the HOMO–LUMO gap of 2.12 ± 0.02 V determined for triarylcorroles, oxidation of the metal was proposed (based on EPR spectroscopy) to precede that of the corrole in the antimony(III) complex of an electron-rich corrole [58]. An intriguing possibility that might fit the data best is that the initially formed species is corrole-oxidized antimony(III), which is transformed into antimony(IV) corrole in an intramolecular process.

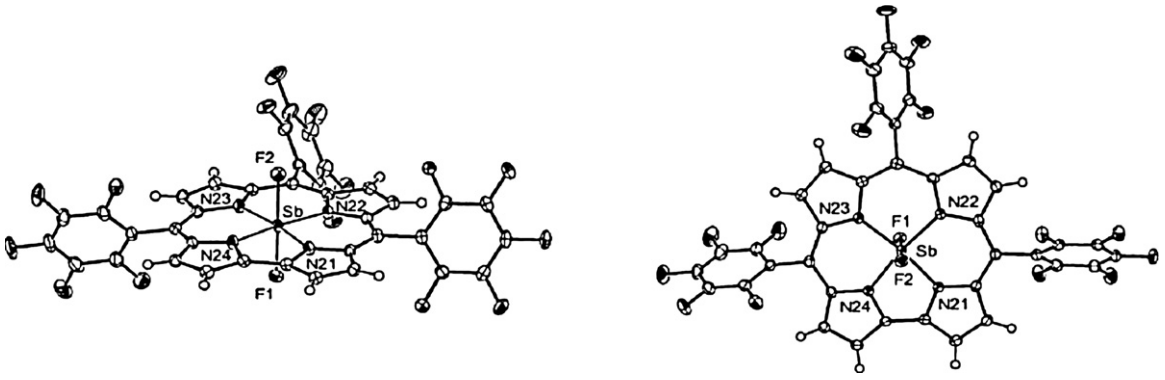

Fig. 6. Molecular structure of Sb(tpfc)$(F)_2$, showing 50% probability thermal displacement parameters at ca. 110 K. Selected bond lengths: Sb–F1 = 1.940(1) Å, Sb–F2 = 1.932(1) Å, Sb–N(pyrrole) average = 1.975 Å. The corrole is essentially planar. Figure was reproduced from Ref. [18], with permission of the copyright holders.

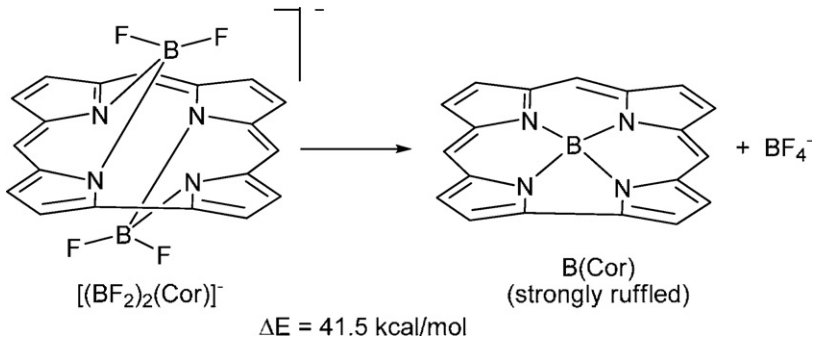

Scheme 9. DFT calculated energetic differences between two plausible boron-corrole complexes.

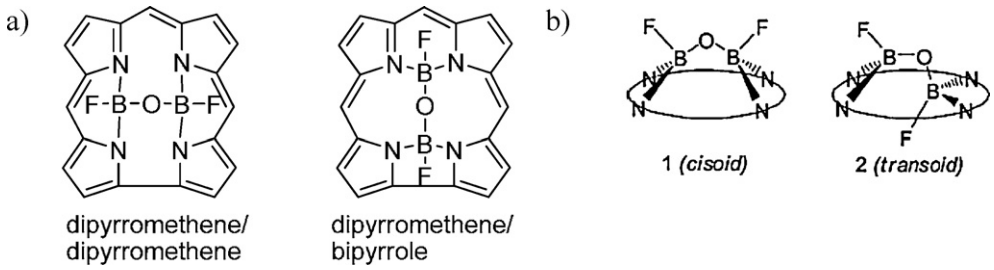

Fig. 7. (a) Dipyrromethene/dipyrromethene and dipyrromethene/bipyrrole regioisomers for diboron corroles illustrated for $[B_2OF_2(cor)]^-$. (b) *Cisoid* and *transoid* geometries, found for corrole and porphyrins, respectively.

7. Boron corroles

In their work on boron porphyrin complexes, Brothers et al. showed that coordination of two boron atoms per porphyrin is possible and that it leads to unusual chemistry regarding both the boron and the porphyrin [59]. The question was whether this binucleating behavior may be extended to corroles as well. The conclusion from density function theory (DFT) study was that the diboron structure is in favor by over 40 kcal mol^{-1} relative to monoboron corrole (Scheme 9), while the absence of evidence for undue structural strain suggested that the reactions of corroles with appropriate boron compounds should be facile [60a].

The reactions of $BF_3{\cdot}OEt_2$ with *meso*-triarylcorroles led to boron corrole complexes indeed, wherein the corrole trianion is coordinated to an FBOBF moiety $[B_2OF_2(cor)]^-$ (the oxygen atom comes from water) and the negatively charged complex is balanced by a diisopropylethylammonium counter-cation. Remarkably, despite of the small size of the N4 core, the corrole ligand can still accommodate two coordinated boron atoms. NMR experiments and X-ray crystallography revealed that each boron atom in the FBOBF unit is coordinated to two adjacent nitrogen atoms in the dipyrromethene sites (dipyrromethene/dipyrromethene). DFT calculations revealed that the alternative structure with coordination of one boron with the dipyrromethene site and the other with the bipyrrole moiety is less favored by 16.1 kcal mol^{-1} (Fig. 7a). Moreover, the FBOBF moiety occupies one face of the corrole in a *cisoid* arrangement (calculated to be 19.5 kcal mol^{-1} lower in energy than the *transoid* isomer), in contrast to the corresponding porphyrin complexes which adopt asymmetric *transoid* geometry (more stable by 15.9 kcal mol^{-1}) (Fig. 7b). The corrole macrocycle is domed, each pyrrole ring is tilted toward a coordinated boron, and the distances between adjacent N atoms in boron corroles are considerably shorter (0.86 Å vs. 1.06 Å) than in boron porphyrins.

A boron-free analog of the above structural motif was obtained as a by-product in the reaction of a free-base corrole with the Vilsmeier reagent [61]. The corrole cation $[(HCCNMe_2)(tpc)]^+$ depicted in Fig. 8 contains an H–C–C–NMe_2 fragment within the corrole core and each carbon atom is attached to two corrole nitrogen atoms. The dipyrromethene/dipyrromethene regioisomer is observed in this case as well, but the two carbon atoms lay above and below the plane of the corrole in a *transoid* fashion. This indicates that a *transoid* geometry might be accessible for boron corroles as well under the right circumstances.

The UV–vis analysis of all synthesized FBOBF derivatives exhibit nearly identical spectra, which are similar to those of free-base *meso*-triarylcorrole derivatives and unlike many transition-metal corrole derivatives whose Soret bands are exceedingly sensitive to peripheral substituents. DFT studies indicate that the substituent sensitivity of the Soret bands of many transition-metal corroles reflects charge-transfer transitions to low-lying empty metal d orbitals or ligand holes. Obviously, a similar situation cannot exist in the electronically saturated boron complexes.

The notable differences between boron corroles and porphyrins were the motivation behind DFT studies on plausible monoboron corrole complexes [60b]. The regioisomer in which the boron is bound to a dipyrromethene adjacent to the bipyrrole (dipyrromethene(A)) is preferred (lowest in energy) relative to the other possible regioisomers in which boron coordinates either in the bipyrrole or in the dipyrromethene site opposite the bipyrrole (Fig. 9). The out-of-plane stereochemistry of the BX_2 group is also in favor for monoboron corrole complexes.

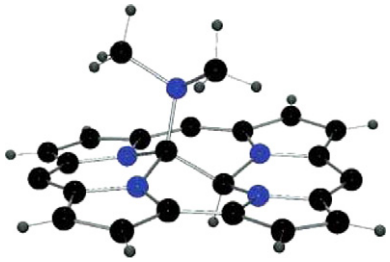

Fig. 8. Molecular structure of $[(HCCNMe_2)(tpc)]^+$ with a dipyrromethene/dipyrromethene structure. Figure was reproduced from the work published in Ref. [61].

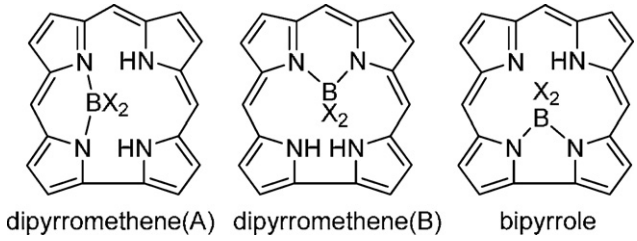

Fig. 9. The dipyrromethene (A), dipyrromethene (B) and bipyrrole regioisomers of $[BX_2(H_2(Cor))]$.

There is only one isolated complex that can be compared with the predicted monoboron corroles: the doubly *N*-substituted free base corrole, in which the carbon atom of a C=O group bridges two adjacent corrole nitrogen (Scheme 10) [12,13]. The crystal structure of that molecule reveals a CO group that is bound to the dipyrromethene adjacent to the bipyrrole site, in analogy to dipyrromethene(A), which is predicted to be most stable isomer of the (so far) hypothetic mononuclear boron corrole.

The first example of a boron hydride corrole complex, $Ph_2B_2H(Cor)$ with a bridging B–H–B unit, was obtained as an unexpected product of the reaction of $PhBCl_2$ with free-base corrole, $H_3(Cor)$ (Cor = TPC, T(4-Me-P)C, T(4-CF_3-P)C) [60c]. ^{1}H NMR spectroscopy revealed some interesting features of this complex: (a) two chemically equivalent phenyl groups, which is consistent with either C_2 or C_s symmetry; (b) B-phenyl resonances that appear at high field as a result of the corrole aromatic ring current; and (c) four doublets for the corrole β-pyrrolic protons. In addition, a broad singlet corresponding to one hydrogen atom at −6.3 to −6.5 ppm was assigned to the hydride, whose presence was also confirmed by MS. The two crystallographic structures confirmed the existence of a bent bridging hydride and both display *transoid* geometry, with the B-phenyl groups on opposite sides of the corrole plane. The X-ray structures do not confirm the exact symmetry suggested by ^{1}H NMR, but they are very close to C_2. The hydrogen atom is displaced 0.62 Å above the mean 4 N plane in the direction of B2, while B2 and B1 are displaced 0.74 and 0.51 Å above and below the mean 4 N plane. The distances of B1–H and B2–H are inequivalent (1.43, 1.13 Å) and the B1–H–B2 angle is 129° (typical bridging B–H–B distances and angles in small molecules). The corrole ring shows a nonplanar distortion with the *meso* carbon atoms in the 5- and 15-positions and their respective flanking pyrrole rings are tilted in opposite directions relative to the mean 4 N plane (Fig. 10).

The mechanism for formation of these intriguing compounds was addressed by DFT calculations, which along with some experimental observations suggest that the reductive process is similar to that observed in porphyrins. But, part of the driving force in the case of corrole appears to derive from protonation of the B–B unit (or capture of a proton during the reduction) to give a unique corrole-encapsulated B–H–B hydride-bridged diboranyl group.

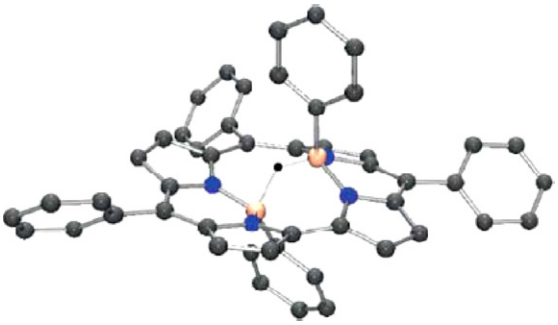

Fig. 10. X-ray structure of $Ph_2B_2H(Cor)$. Figure was reproduced from Ref. [60c], with permission of the copyright holders.

8. Photophysical properties

8.1. Absorbance

The electronic spectra of 5,10,15-triarylcorroles are similar to their analogous 5,10,15,20-tetraarylporphyrins, consisting of an intense near-UV band (called Soret band, which is usually single and sharp) and several visible (Q) bands. In most metallocorroles, the Q bands are stronger and the Soret bands somewhat weaker than in corresponding porphyrin complexes. This may be appreciated by the spectra shown in Fig. 11, which further stress that gallium(III) complexes with trianionic corrolato ligands are the analogs of dianionic-porphyrinato zinc(II) complexes. An identical relationship exists between Al^{III} corroles and Mg^{II} porphyrins [62].

In addition, corroles chelated by non-transition elements display some interesting spectroscopic and photophysical properties (such as much higher fluorescence quantum yields, see Fig. 11), which suggest that they could be attractive alternatives to porphyrins in dye-sensitized photovoltaic cells and photodynamic therapy and for proposed use in photon-actuated molecular logic devices. High quantum yields of S_1–S_0 fluorescence, dual S_2–S_0 and S_1–S_0 fluorescence, together with facile synthetic access to water-soluble derivatives, are among the features required for such applications.

8.2. Fluorescence

A most prominent feature of the non-transition metal complexes of corroles is their strong fluorescence. Interestingly, the fluorescence intensity of corroles is generally (and most so for tpfc derivatives) [38] much larger than that of porphyrins and other related macrocycles. The variables that affect this feature were studied by comparing the fluorescence quantum yields (ϕ_f) of various free-base corroles and their corresponding main group complexes (Table 4). The quantum yield of corrole **1** $[H_3(tpfc)]$ is 0.20 and increases to 0.35 by deprotonation (note that the pka of its NH proton is 5.2!) [63] as to form $[H_2(tpfc)]^-$ (entry 4). Metal-

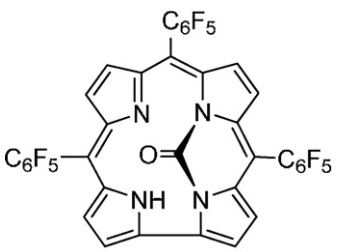

10

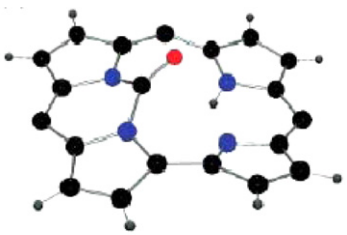

Scheme 10. Formal drawing and molecular structure of the (chiral) corrole **10**, with a dipyrromethene (A) structure. Figure was reproduced from the work published in Refs. [12,13].

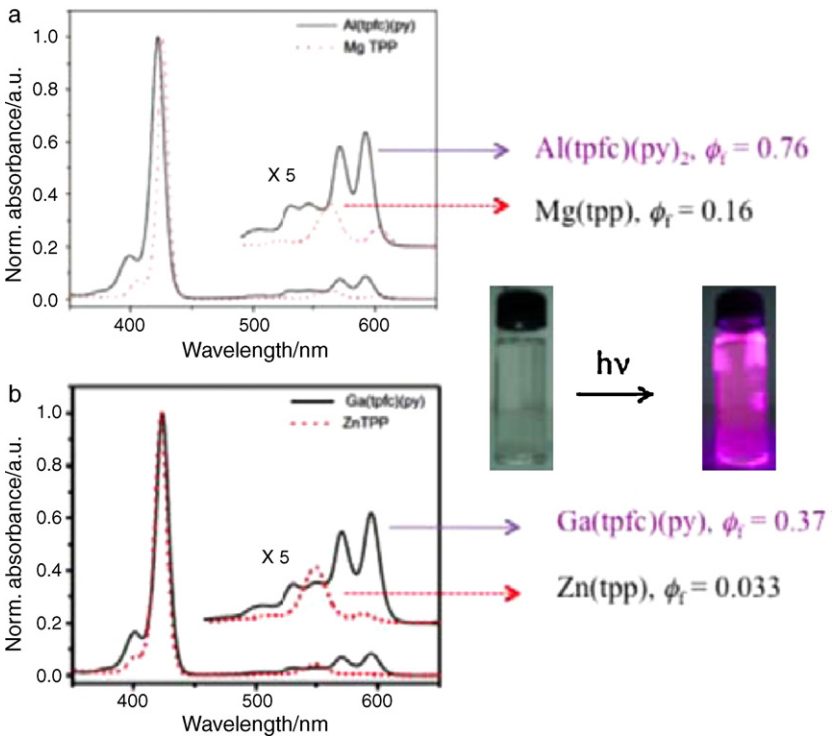

Fig. 11. Absorption spectra (normalized to the maxima of the Soret bands) of (a) Al(tpfc)(py) compared with Mg(tpp) and (b) Ga(tpfc)(py) compared with Zn(tpp), Figure was reproduced from Ref. [62], with permission of the copyright holders. Also shown are the fluorescence quantum yields of these complexes and the strong fluorescence of a solution of Al(tpfc)(py) that is as dilute as to appear colorless under regular light.

lation of **1** by gallium and especially by aluminum leads to a large increase in ϕ_f; from 0.20 to 0.37 for [Ga(tpfc)(py)] and as high as 0.76 for [Al (tpfc)$(py)_2$] (entries 5 and 8). This is quite in contrast to 5,10,15,20-tetraphenylporphyrin [H_2(tpp)], where metallation by zinc(II) reduces ϕ_f from 0.13 to 0.033 (entries 1 and 2).

The increase in the corrole quantum yield upon metallation and deprotonation can be explained in part by ring distortion variations. In the free-base corrole three protons accommodate the core. The pyrrole rings must hence distort from planarity (the mean plane deviation is 0.202 Å), whereas replacement of either one (by deprotonation) or all these protons by metallation allows the pyrroles to adopt a near planar geometry (the mean plane deviation for Ga(tpfc)(py) is 0.136 Å). The suggestion that planar structures emit even more efficiently is further supported by the observation that the 6-coordinate bis-pyridine gallium(III) corrole (entry 7) has an even higher fluorescence quantum yield (0.47). The mean plane deviation for the related bis-pyridine compound, 3,17-$(NO_2)_2$-Ga(tpfc)$(py)_2$, is as low as 0.063 Å.

The ϕ_f of 0.76 for Al(tpfc)$(py)_2$ (entry 8) is in fact a record value for oligopyrrolic macrocycles. The 27% increase (from 0.37 to 0.47) in ϕ_f upon converting the 5-coordinate Ga(tpfc)(py) into the hexa-coordinated Ga(tpfc)$(py)_2$ (entries 5 and 7) indicates that the reason for the very high fluorescence quantum yield of Al(tpfc)$(py)_2$ is a combination of two processes: not supporting intersystem

Table 4
Absorption, emission, and fluorescence quantum yields for corroles and reference porphyrin (n.r. = not reported).[a]

Entry	Compound	Absorption, λ_{max} [nm] ($\varepsilon \times 10^{-4}$ M^{-1} cm^{-1})	Emission, λ_{max} [nm]	Fluorescence quantum yields (ϕ_f)	Ref.
1	H_2(tpp)	419 (26.7), 592 (1.0), 650 (1.0)	654, 720	0.13	[38,50]
2	Zn(tpp)	423 (45.2), 588 (0.3)	600, 648, 715	0.033	[38,50]
3	H_3(tpfc), 1[b]	408 (11.4), 602 (0.9)	648, 622, 704	0.20	[38,50]
4	[H_2(tpfc)]$^-$[c]	n.r.	628	0.35	[38]
5	Ga(tpfc)(py)[b]	424 (28.3), 596 (2.4)	602, 656	0.37	[50]
6	Ga(tpfc)(py)[d,e]	424 (27.0), 594 (2.1)	606, 620, 660, 680	0.40	[50]
7	Ga(tpfc)$(py)_2$[f]	626 (21.4), 610 (1.8)	620, 680	0.47	[50]
8	Al(tpfc)$(py)_2$[d]	432 (29.4), 620 (3.7)	627, 689	0.76	[50]
9	Al(corrolin)[d]	378 (3.5), 616 (2.9), 644 (4.0)	660, 727	0.62	[50]
10	(N^{21}-picolyl)H_2(tpfc)	n.r.	630, 684	0.26	[38]
11	(N^{21}-benzyl)H_2(tpfc)	n.r.	630, 682	0.30	[38]
12	Ge$(tpc)_2$(O)	399 (36.3), 528 (1.34), 567 (2.1), 598 (2.4)	n.r.	0.033	[20]
13	Ge(tpc)(OMe)	412 (16.0), 522 (0.7), 560 (0.9), 590 (2.1)	n.r.	0.14	[20]
14	2,3,8,12,17,18-hexabromo-Ge(tpc)(OMe)	428 (24.8), 538 (12.1), 578 (2.5), 603 (3.8)	n.r.	0.005	[20]

[a] Under Ar, with ϕ_f = 0.13 for H_2(tpp) as reference.
[b] In toluene only.
[c] A solution of H_3(tpfc) in the presence of Et_3N.
[d] In 5% pyridine/toluene.
[e] A mixture of mono- and bis-pyridine complexes.
[f] In 100% pyridine (only Ga(tpfc)$(py)_2$).

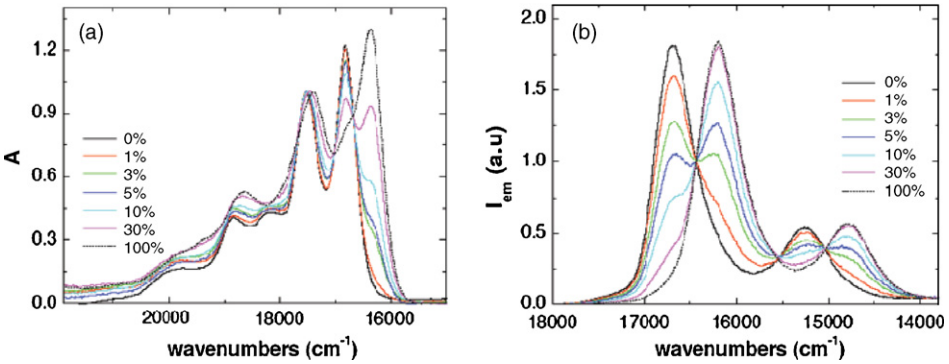

Fig. 12. (a) Absorption and (b) emission spectra of Ga(tpfc)(py)$_n$ in benzene as a function of added pyridine. Figure was reproduced from Ref. [52], with permission of the copyright holders.

crossing of the singlet excited state to the triplet (ISC) (a light metal) and a large structural rigidity of the hexa-coordinated complex, reducing the probability for non-radiative relaxation (also called internal conversion, IC). These seem to be the main factors of the earlier mentioned superior feature of aluminum corrolin whose ϕ_f is almost twice as large as that of the natural pigment, chlorophyll-a (0.62 vs. 0.32) (entry 9). The fluorescence quantum yields of *N*-substituted corroles obtained from corrole **1** (entries 10 and 11, Scheme 3) are also quite high; 0.26 for N^{21}-picolyl-tpfc and 0.30 for N^{21}-benzyl-tpfc, which indicates that corroles may be attached by one of their nitrogen atoms to a variety of solid supports without losing useful photophysical properties. Consistent with expectation, corroles with *meso*-substituents that are either more flexible such as heptafluoropropyl or contain heavy atoms such as in dichlorophenyl possess a much lower quantum yield [50,64].

The fluorescence quantum yield of the non-brominated germanium(IV) corroles (Table 4, entries 12 and 13) is also higher than the corresponding porphyrins, but still lower than of aluminum(III)- and gallium(III)-(tpfc), because of a nonplanarity of the macrocycle in the latter (5-coordinate with domed corrole). Importantly, Ge(tpc)$_2$(O) and Ge(tpc)(OMe) were shown to be phosphorescent at 77 K, with emission observed in the 760–840 nm region. Their excited state lifetime is about 30 ms at 77 K, while the hexabrominated complex decayed ten times more quickly, indicating a much faster inter-system crossing process due to the heavy atom effect. Interestingly, iridium(III) corroles are phosphorescent even at ambient temperature with emission of 788–795 nm and β-pyrrole bromination induced a red shift without a reduced lifetime [65].

Fluorescence from the second excited singlet states in the Soret-excited of two metallated corroles, Al(tpfc)(py) and Ga(tpfc)(py), has first been observed only quite recently [62]. The excited state dynamics have been investigated in direct measurements using femtosecond fluorescence upconversion methods. The S_2 excited states relax to the S_1 states on a sub-picosecond time scale with quantum efficiencies in the 0.8–0.9 range. The rate of S_2 population-decay rate equals the rate of S_1 population-increase, and there was no evidence of a significant heavy-atom induced S_2–T_n ($n > 2$) intersystem crossing in the gallium(III) compared with the aluminum(III) corrole. The radiative and nonradiative decay rate constants for the S_2 states of these corroles are consistent with smaller transition moments for S_2–S_0 radiative decay and substantially increased radiationless transition rates, compared with similar metalloporphyrins.

8.3. Ground and excited-state dynamics

The equilibrium constants between the 5-coordinate and the 6-coordinate aluminum(III) and gallium(III) corroles were determined in mixed benzene-pyridine solutions [52]:

$$M(tpfc)(py) + py \rightleftarrows M(tpfc)(py)_2$$

Both complexes are 5-coordinate when dissolved in noncoordinating solvents (benzene, toluene), and ground-state equilibrium between the five- and six-coordinate species is established when pyridine is added to the solution. In pure pyridine the 6-coordinate species is exclusively formed: addition of increasing amounts of pyridine to a benzene solution (until all benzene is fully replaced by pyridine) for Ga(tpfc)(py)$_n$ changed the absorption and fluorescence emission spectra as illustrated in Fig. 12. A distinct shift also exist for Al(tpfc)(py)$_n$ but the 6-coordinate complex is fully formed at much lower pyridine concentration. In both corroles, the six-coordinate species absorb and emit further to the red relative to the 5-coordinate complexes.

By measuring the difference between the energies of the ground and excited electronic states using the Q- and Soret-band spectroscopic shifts, it appears that stabilization produced by adding a second pyridine ligand is smaller for the gallium(III) corrole than for the aluminum(III) corrole; and that is smaller in the S_2 states of both molecules than in their S_1 states. The ground-state equilibrium constants reveal that the 6-coordinate aluminum(III) is considerably more stable than the gallium(III) complex. The corresponding values of the ground-state association constant, K_a, equals to 135 M^{-1} and 1.0 M^{-1} at 295 K for Al^{III} and Ga^{III}, respectively. In other words, the aluminum(III) acts as significantly stronger Lewis acid than gallium(III) in these corroles, which is also reflected in the earlier discussed metal–N(pyridine) bond lengths.

The fluorescence lifetimes of the gallium(III) corroles are significantly shorter that those of the corresponding aluminum(III) compounds, almost exclusively due to their larger S_1 radiationless decay constants. This difference in the radiationless decay rates of the two metallocorroles is consistent with a faster rate of S_1–T_1 intersystem crossing in the gallium(III) compound due to its enhanced heavy-atom-induced spin–orbit coupling. Curiously, however, again due primarily to differences in their radiationless decay rates, the S_1 lifetime of the 6-coordinate aluminum(III) corrole (6.60 ns in pyridine) is somewhat shorter that that of the 5-coordinate species (7.34 ns in benzene), whereas the lifetime of the S_1 state of the 6-coordinate gallium(III) compound (3.45 ns in pyridine) is slightly longer that its 5-coordinate counterpart (3.04 ns in benzene).

Temporal S_1 fluorescence decay profiles of Ga(tpfc)(py)$_n$ system were measured in mixed benzene-pyridine solutions as a function of the concentration of pyridine added to benzene solutions of the (initially) 5-coordinate corroles. These experiments revealed that the fluorescence profiles of the corroles in those mixtures are all biexponential due to dissociation of the 6-coordinate species in the

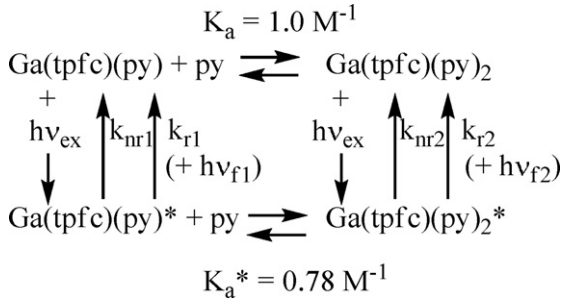

Scheme 11. A kinetic model of the coordination of Al(tpfc)(py)$_n$ and Ga(tpfc)(py)$_n$ (n = 1, 2).

excited state, leading to establishment of excited-state dissociation association equilibrium.

The rate constants for the pyridine association and dissociation processes for the Ga(tpfc)(py)$_n$ system in the excited state are: ka* = 2.3 × 10^8 M^{-1} s^{-1} and kd* = 2.9 × 10^8 s^{-1}, leading to a value for the excited-state association equilibrium constant of Ka* = 0.78 M^{-1} (Scheme 11). These rate constants are the first measured for excited state ligand association-dissociation reactions in metallocorrole systems. This information is of practical importance as well, such as for inducing light-driven ligand exchange in substitution-inert complexes.

8.4. Photoexcited triplet state properties of corroles

Many light-induced processes in metallocorroles may proceed via transient paramagnetic states. Time-resolved electron paramagnetic resonance (TREPR) spectroscopy, combined with selective laser light excitation, is a suitable tool to provide unique information on the nature of corrole complexes bearing different core ions and different axial ligands [40]. The value and the sign of the zero-field splitting (ZFS) parameter D is an important feature of the corrole. Analysis of the TREPR spectra of free-base corrole and its chelates points toward a negative sign of D, which is unusual for planar and nearly planar tetrapyrrolic compounds. This phenomenon occurs since corroles have lower symmetry relative to porphyrins and is further amplified by the asymmetric π-electron withdrawal effect generated by the perfluorinated aryl rings. DFT calculations confirmed this assumption and demonstrated that the electron spin density on the inner nitrogen atoms in corroles is much smaller compared to porphyrins [38]. The negative sign of D is a result of the "stretch" of the triplet molecular orbitals along one of the molecular axes, which enforces the corresponding electron spins to align in a head-to-tail configuration. This allows an explanation for the unusual TREPR spectroscopic polarization patterns observed in corroles differing by core metal ion and symmetry. Two gallium(III)–corrole complexes, the brominated Ga(tpfc-Br$_8$)(py) (**3**) and the non-brominated Ga(tpfc)(py) (**2a**) (Scheme 6) were compared via examination of the effect of the corrole macrocycle bromination on its photoexcited triplet state parameters. Bromination of the gallium(III) corrole results in the inversion of the spectroscopic polarization pattern: from a/e (absorption/emission) polarization pattern observed in the nonbrominated gallium corrole **2a** to e/a (emission/absorption) pattern in the brominated gallium complex **3**. This effect can be interpreted in terms of the negative D sign in the corroles. Evidently this is the case, and the overpopulation of the Z-axis is reflected by the e/a polarization pattern of the brominated corrole spectra. A larger $|D|$ value was observed for the brominated Ga–corrole compared to nonbrominated one. With the assignment of a negative sign D, the dominant intersystem crossing (ISC) pathways are evaluated. Spectroscopic line shape analysis revealed that in the brominated gallium corrole **3**, the out-of-plane triplet sublevel is overpopulated ($A_Z > A_X$, A_Y), while in nonbrominated gallium corrole **2a**, the in-plane triplet sublevels are preferentially populated ($A_X, A_Y \gg A_Z$). The differences in the photophysical properties of the corroles are attributed to the heavy atom effect upon corrole skeleton bromination, which enhances the spin–orbit coupling strength in the brominated complex, thus affecting its ISC and ZFS parameters.

Other publications showed that the free-base corrole and the corrole complexes containing the ions Al^{III}, Sn^{IV}, Sb^{III}, and Sb^{V} display the same spectroscopic polarization patterns [19,66]. That means there is no indication of a heavy atom effect, i.e., changes in the ISC parameters due to the insertion of a heavy element into the coordination core of the molecule. This points to a similar population ratio of the triplet sublevels in the free-base corrole and in the different metallocorrole complexes. These unusual results were explained by the experimentally determined domed structure of the penta-coordinated corroles, which decreases the d–π electronic interaction between the central metal and the corrole ring. A comparison of the TREPR spectra of free-base corrole with Ga(tpfc-Br$_8$)(py), Ga(tpfc)(py), Al(tpfc)(py), Sn(tpfc)(Cl), Sb(tpfc)(py), Sb(tpfc)(O), Sb(tpfc)(F)$_2$ verifies a regular trend in the corrole structure–function relationship.

9. Applications

Recent accounts on the applications of metallocorroles have been recently published [9]; hence this section focuses only on those relevant to main group chelates. The emphasis is on applications that take advantage of the unique photophysical properties of these complexes for catalyzing organic reactions, approaches important for alternative energy resources, and in medicine-oriented projects.

9.1. Catalysis by antimony corroles

All three antimony complexes; Sb(tpfc)(py), Sb(tpfc)(F)$_2$ and Sb(tpfc)(O) (**9a**, **9b**, **9c**, Scheme 8) display high catalytic activity for the photo-induced oxygenation of thioanisole by molecular oxygen, with the best results achieved in alcoholic solvents (no reaction in benzene). The corresponding sulfoxide was the only product regardless of the catalyst used, and no further oxidation to the sulfone was obtained. The catalytic efficiency was in the order of Sb(tpfc)(F)$_2$ > Sb(tpfc)(O) > Sb(tpfc)(py). With only 0.02 mol% of Sb(tpfc)(F)$_2$, full conversion of thioanisole to its sulfoxide (5000 catalytic turnovers) was obtained without any indications for catalyst bleaching. When thioanisole was replaced by diphenylsulfide (which is known to be inert toward oxidation by singlet oxygen), no reaction took place. This strongly suggests that the antimony corroles are efficient photosensitizers of molecular oxygen and that the thus formed singlet oxygen is the active oxidant.

Sb(tpfc)(F)$_2$ was further examined as a potential photocatalyst for the oxidation of hydrocarbons. The selectivity of CH vs. C=C bonds was absolute; styrene remained unreacted and only the allylic CH bonds of cyclohexene and cyclooctene were oxidized. This is also consistent with the reactivity profile of singlet oxygen, which is characterized by very efficient "ene" reactions. Out of the three non-olefin-containing substrates that were examined; ethylbenzene, admantane and cumene, only the latter was oxidized. The selectivity reflects the mechanistic aspects of reactions that proceed with C–H abstraction as the rate-limiting step, with singlet oxygen as the oxidizing reagent. Control reaction revealed that when any of the constituents required for efficient formation of singlet oxygen is omitted, no reaction of any of the substrates took place. Another important issue is selectivity: the corresponding hydroperoxides were obtained as the sole products in all cases

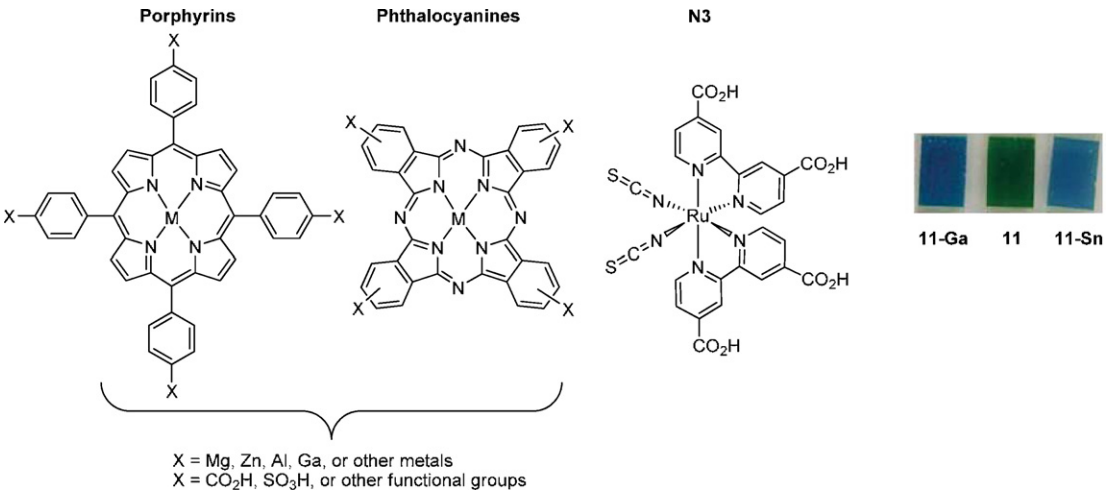

Scheme 12. Metal complexes used in dye-sensitized solar cells and pictures of the corroles-bound nanoporous TiO_2 electrodes.

(determined by NMR). It is important to note that Sb(tpfc)$(F)_2$ was not destroyed or modified to any appreciable extent (monitored by TLC and UV–vis) and when the ratio of substrate:catalyst was increased to 2000:1, up to 78% conversion was obtained. These results outperform all previous reports in terms of absolute catalytic turnover numbers and selectivity. The apparent potential of main group corroles as photosensitizers for biological applications that rely on singlet oxygen, as well as for conversion of light to electricity, are likely to be further advanced in the near future.

9.2. Dye sensitized solar cells (DSSC)

Dye-sensitized solar cells (DSSC) appear to be very promising devices for conversion of solar energy into electricity. The most intensively investigated sensitizers are derivatives of ruthenium(II) bipyridines and porphyrinoids. The porphyrinoids are attractive because it is easy to tune their photophysical properties by substitutions on their molecular frameworks and/or via variation of the central metal ion. Since the frontier orbitals of the corrole are at higher energy than those of analogous porphyrins [55], their application as sensitizers in DSSC was examined. Corrole **11** and its gallium(III) (**11-Ga**) and (chloro)tin(IV) (**11-Sn**) (Fig. 13) complexes were chosen because of their structural similarity to the best performing dyes displayed in Scheme 12 [11b], and because their sulfonic acid head groups may be used for binding to nanoporous TiO_2 electrodes.

The incident photon to current efficiency (IPCE) spectra of the corroles on nanoporous TiO_2 revealed substantial differences in the efficiencies of the dyes: **11-Ga** ~ **11** ≫ **11-Sn**. The absorbed photon to current efficiency (APCE) plots were in the same order as their IPCEs, indicating that the variations in efficiencies of these dyes are apparently not due to differences in light absorption. The low efficiency of the **11-Sn** based DSSC was deduced to reflect the inability of its excited state to inject electrons into the TiO_2 film. With a > 0.5 V more positive reduction potential of the **11-Sn**$^{+/0}$ couple than those of **11-Ga**$^{+/0}$, **11**$^{+/0}$ and **N3**$^{+/0}$, the **11-Sn** excited state is indeed not nearly as potent a reductant as the other. These results suggest that certain selectively substituted corroles may perform well as components of DSSC. In fact, the TiO_2-adsorbed **11** and **11-Ga** display cell efficiencies under AM 1.5 illumination that are already about half that of a standard **N3**-sensitized solar cell [(*cis*-bis(4,4′-dicarboxy-2,2′-bipyridine)dithiocyanato ruthenium(II)] and larger than typical values for cells with other tetrapyrrolic sensitizers. The properties of the corrole-TiO_2 solar cells clearly reveal that the reducing power of the singlet excited states of the free-base **11** and **11-Ga** corrole is sufficiently high for efficient injection into the TiO_2 conduction band (this is not the case for **11-Sn**) and that corroles (and also other porphyrinoids) with excited-state reduction potentials substantially more positive than roughly −1.0 V likely will not perform well in DSSC based on TiO_2. The large advances in corrole synthesis assure that many other derivatives will be available for such research. For example, corroles bearing carboxylate rather than sulfonate head groups [12] may assure tighter binding and likely also more efficient electron transfer rates.

9.3. Chemiluminescence enhancement and energy transfer

Another recently reported utilization of the photophysical properties focuses on the luminol-based chemiluminescence assay, routinely used for measuring both extracellular and intracellular (luminol penetrates cellular membranes) levels of reactive oxygen species (ROS, such as H_2O_2, $O_2^{-\bullet}$ and •OH) [54]. The emission of luminol at 420–450 nm is not ideal for most biological applications, therefore enhancing the CL of luminol and recording the output signal of light at tissue-penetrating wavelengths is very important. A logical and relatively easy way for achieving the latter goal is by the CET process, relying on acceptors that efficiently absorb energy in the near-UV (where luminol emits) and release it (*via* fluorescence) at significantly longer wavelengths.

The broad chemiluminescence (CL) spectrum of luminol overlaps very much with the absorption of the water soluble and bipolar free-base corrole **11** (Fig. 13) and its gallium(III) (**11-Ga**) and aluminum(III) complexes (**11-Al**), while these corroles

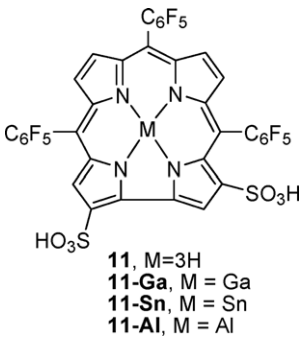

Fig. 13. The structure of the amphiphlic and bipolar corrole **11** and its metal complexes, used for many applications.

emit at tissue-penetrating wavelengths (600–750 nm). In the presence of 10 mol% of **11-Ga**, the CL of luminol was dramatically decreased at 400–440 nm, which may safely be attributed to the strong absorption of the corrole. The emission at λ_{max} of 625 nm under these conditions clearly testifies that **11-Ga** was excited *via* non-resonance energy transfer by the luminol's CL. A CET efficiency of 2% was determined, which is quite large considering the low concentrations of the molecules and the fact that they are not bound to each other by any strong forces. The analogues porphyrin, H_2TPPS, did not emit any light at the expected wavelengths (600–760 nm) at the same conditions, despite its intense Soret band at 420 nm. The best results were achieved by using **11-Al**: a CET efficiency of 10% and an about *threefold increase in the CL of luminol*. The results reveal that **11-Al** acts as a strong CL enhancer and that the excitation of **11-Al** occurs *via* efficient (non-resonance) energy transfer by the luminol's CL. Mechanistic investigations revealed two main factors that determine the above properties: the fluorescence quantum yield of the acceptors is apparently one key factor in determining the CET efficiency in this system, with the order of aluminum(III) corrole > gallium(III) corrole > free-base corrole > free-base porphyrin > zinc(II) porphyrin. The observed CET efficiency varies in exactly the same order indeed, i.e., **11-Al** > **11-Ga** > **11** > H_2TPPS and ZnTPPS. The other factor, important for enhancing the CL of luminol, is the redox potential. ZnTPPS was found to increase the CL of luminol as efficiently as **11-Al**, while H_2TPPS, **11-Ga** and **11** had no effect. Utilization of *p*-iodophenol, the most prominent CL enhancer in the horseradish peroxidase catalyzed luminol–H_2O_2 reaction, increased the CL intensity in the Cu/luminol/H_2O_2 system as well and the trend for CL enhancement of luminol was established to be **11-Al** ∼ ZnTPPS > *p*-iodophenol ≫ **11-Ga**, H_2TPPS and **11**. The clue for the origin of this observation is their correlation with the redox potentials of these compounds, which are 0.52, 0.65, 0.61, ≥0.7, and 1.1 V (vs. Ag/AgCl), for **11-Al**, ZnTPPS, *p*-iodophenol, **11-Ga**, and H_2TPPS, respectively. The combined features of **11-Al** are that its CET process with luminol occurs in 10% yield without the need of covalently binding the corroles to the CL donor and that the CL-excited corroles emit light at wavelengths that are tissue-penetrating, crucial requirements for probes that may be applied in biology and biotechnology. This is one main advantage of the corrole relative to fluorescein, which is also a good enhancer (less than **11-Al**) and acceptor (better than **11-Al**) of luminol's CL, but emits at much shorter wavelengths (λ_{max} of 535 nm, when tested under identical reaction conditions).

9.4. Corrole:protein conjugates

The 2,17-bis-sulfonato-5,10,15-(tpfc) (**11**) and its gallium(III) (**11-Ga**), manganese(III) and iron(III) (Fig. 13) complexes spontaneously form tightly bound conjugates with proteins, due to the amphiphilicity and the bipolarity of the corrole [67,68]. The photophysical properties of that free-base corrole and its main group complexes suggests that they could have a great potential for many medicine-oriented applications. The first protein that was thoroughly examined is the most abundant one in blood plasma: human serum albumin (HSA), which plays a variety of roles in many biological processes. Spectroscopic experiments on **11-Ga** revealed that its Soret band shifts from 424 to 430 nm when treated with increasing amounts of HSA. The effect of HSA on the corrole-based fluorescence is a reduction in intensity at tenfold excess corrole (40% and 60% for **11** and **11-Ga**, respectively), followed by an increase (to 60% and 130%, respectively, of the initial intensity) at equimolar ratio. These results were interpretated by self-quenching when many corrole molecules are bound to the same protein, while the restoration of fluorescence intensity is consistent with specific binding resulting in less degrees of freedom. Indications for an extremely strong 1:1 association, as well as other only slightly weaker association constants for multiple corroles/HSA conjugates, were obtained by circular dichroism (CD) spectroscopy as well. The CD spectra at long wavelengths (λ > 360 nm) nicely confirm that the corroles are located within the chiral environment pockets provided by the protein residues. HPLC profiles of the conjugates and selective fluorescence quenching of the single tryptophan (Trp) present in HSA were also interpreted in terms of multiple corrole:HSA binding sites, of which the strongest one has a $K_d \ll 10^{-8}$ M. It is apparent that the corroles will be fully bound to HSA under physiological conditions. The preferred (1:1) binding site is likely to be the one that also bind hemin [69], as it is within the Förster quenching calculated distance from the unique Trp [67].

Corrole **11** and its gallium(III) (**11-Ga**) and manganese(III) complexes were also determined to spontaneously bind transferrin (Tf) in both its iron-free apo form (apoTf) and the iron-bound holo form (holoTf) [70]. Transferrin is an excellent candidate for specific targeting of molecules of interest to cancer cells and to the brain, thus the corrole-transferrin conjugates might be utilized for targeting these corroles to cells that express the transferrin receptor. Dilution experiments measured by fluorescence revealed very small dissociation constants of 2×10^{-7} M and 3×10^{-8} M for **11-Ga** with apoTf and holoTf, respectively and $<10^{-9}$ M for **11** with both protein. Transferrin concentration in the body is $2.5–4 \times 10^{-5}$ M, therefore the dissociation constants established for the corroles demonstrate that the interactions could be physiologically relevant. One limitation that still needs to be resolved is the strong association of the corroles to serum albumin. Nevertheless, the binding of the corroles to both proteins is a reversible process, which is not the case for most if not all other metallodrugs. This, together with the similar binding of apoTf and holoTf, clearly indicate that the corroles do not occupy iron binding sites of the protein, which is another feature that distinguishes these molecules from other metal-containing drugs.

9.5. Imaging for determining cellular uptake

The first utilization of corroles for appreciating cellular uptake was reported in 2006 [71], after the spontaneous and very strong association of **11-Ga** (Fig. 13) with serum albumins was discovered [67,68]. That investigation revealed that cell entry is protein-mediated and correlated with the affinity for association of the corrole with different protein. For instance, although the dissociation constants of **11-Ga** from its spontaneously formed bioconjugate with apo- and holo-transferrin are in the range of 10^{-7} to 10^{-8} M, human serum albumin can still outcompete the corrole from transferrin conjugates [70]. The association of **11-Ga** with a specifically designed breast cancer delivery protein is however even stronger. This was proven by checking the effect of free heregulin (HER) on cell entry of **11-Ga** conjugated to BSA and HER-tagged protein, revealing that free HER had a negative effect only on the latter [71].

Manganese(III) and iron(III) complexes of corrole **11** (**11-Mn** and **11-Fe**) were found to be highly promising catalysts for decomposition of reactive oxygen and nitrogen species (ROS and RNS, respectively) in pure chemical systems. This includes peroxynitrite (PN) [72], H_2O_2 (catalase-like activity) [68], and $O_2^{-\bullet}$ (SOD-like activity) [73]. Biochemical investigations revealed that **11-Fe** is a very efficient antioxidant regarding the reaction between low density lipoproteins (LDL) and peroxynitrite, while **11-Mn** acted as a pro-oxidant under identical conditions. Oral administration of these complexes to mice engineered to develop atherosclerosis revealed that **11-Fe** attenuated the development of atherosclerotic lesions more efficiently than any other compound reported to date. The protective properties of metal complexes with both

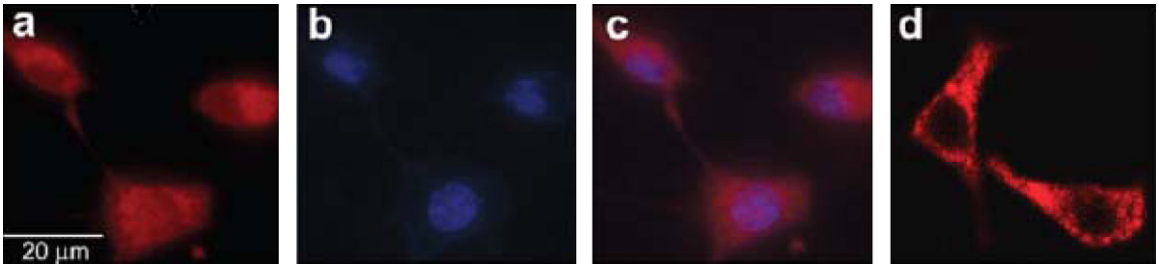

Fig. 14. Cellular uptake of the fluorescent corrole **11-Ga** by RIN-m cells: (a) corrole detection by fluorescence; (b) nuclei staining by DAPI; (c) merged images of panels a and b; and (d) confocal fluorescence image. Figure was reproduced from Ref. [74], with permission of the copyright holders.

positively and negatively charged corroles were also tested against peroxynitrite-induced cytotoxicity in insulin-producing beta cells [74]. All these transition metal complexes are, however, not fluorescent and their uptake in cells and/or organs of interest is not easily determined. The gallium(III) complex **11-Ga** was hence utilized for addressing whether corroles **11-Fe** and **11-Mn** (with sulfonic acid head groups) possess the capacity to penetrate live cells and accumulate therein (as they might actually be rejected by the negatively charged cell membrane). **11-Ga** is the structural analogue of these complexes and has no catalytic antioxidative ability but can be easily traced due to its intense fluorescence. Nuclei staining of insulinoma RIN-m cells by DAPI (4=,6-diamidino-2-phenylindole) and the detection of **11-Ga** by fluorescence microscopy of the same cells (panels a–c, Fig. 14) clearly show that the corrole easily penetrates cell membranes, accumulates in the cytoplasm, and remains excluded from the nucleus as exemplified by confocal microscopy (panel d, Fig. 14) [74]. These examinations clearly indicate that even corroles with negatively charged head groups are eligible agents for intracellular cytoprotection, evidently *via* protein-mediated internalization. The positively charged complexes could not be examined by this method because fluorescent analogue of these corroles have not yet been developed.

9.6. Imaging of whole animals

Small animal imaging has recently emerged as a preclinical tool to perform advanced research more efficiently than ever before. It allows for the reduction of the R&D costs for the development of novel diagnostic and therapeutics, and also provides better understanding about diseases' pathways and biological processes in medical and pharmaceutical research. Optical imaging has several advantages compared to other non-invasive technologies (Ultrasound, CT, MRI, PET, SPECT) since it can offer simultaneous monitoring of multiple targets or molecular pathways, and is often cheaper, simpler and less harmful. Whole body imaging techniques that rely on luminescence have been utilized for investigating tumor progression and metastasis, while gene expression and cell tracking in intact animals is possible because light-emitting molecules may be detected with high sensitivities even in heterogeneous media. Particularly, fluorescence life time imaging (FLIM) can be used as a very useful tool for localizing diseased tissues targeted by fluorophores. What is more, it allows one to identify the functional status around the fluorophores since the fluorescence lifetime can be changed by environmental aspects, such as extracellular vs. intracellular pH, blood flow, tissue oxygen, and temperature. Farkas and co-workers described a scanning fluorescence life time imaging (SFLIM) system that provides a large field of view (LFOV), using a femtosecond (fs) pulsed laser, for multi-mode optical imaging of small animals [75]. This system was used for *in vivo* detection of the fluorescence lifetime regions of injected corroles to mice, taking advantage of the intensely fluorescent **11-Ga**, which spontaneously assembles with carrier proteins to undergo cell entry [76]. *in vivo* experiments that were carried out by injection of **11-Ga** and the carrier protein into mice implanted with human breast cancer tumors showed that **11-Ga** fluorescence exhibited a broad systemic distribution throughout most of the mouse. On the other hand, HerGa (a non-covalent conjugate between the breast cancer-targeted cell penetration protein HerPBK10 and **11-Ga**) showed a preferential accumulation in the tumors and a much lower distribution to extratumoral areas compared with free **11-Ga** (Fig. 15a). Another important observation is that HerGa accumulates at tumor sites within minutes after administration, as indicated by images taken at sequential time points in real time soon after the tail vein injection (Fig. 15b).

9.7. Cancer

9.7.1. Targeted gallium corrole for tumor elimination

The leading causes of death are heart disease and cancer, with the latter in emerge during the years and on the track to overtake the former and become number one. A combination of the breast cancer-targeted cell penetration protein (HerPBK10) and the sulfonated gallium(III) corrole (**11-Ga**) was originally examined for investigations that focused on uptake and possible damage to cellular models of breast cancer. These *in vitro* studies showed that HerGa specifically bound and entered $HER2^+$ (heregulin positive) but not $HER2^-$ (heregulin negative) human cancer cells in separate cell cultures, and induced $HER2^+$ but not $HER2^-$ cell death [71]. Later studies showed that $HER2^+$ cells can even be targeted in a mixed culture of $HER2^+$ and $HER2^-$ cells [76]. These observations together with the earlier described imaging results show that the corroles spontaneously assemble with the carrier protein, which provides both the targeting and penetration required for effective corrole delivery. According to this hypothesis, the corroles will induce toxicity to the target cells only after delivery and uptake by the carrier, thus avoiding detrimental effects to non-targeted cells. Selectivity of *in vivo* HerGa (HerPBK10–**11-Ga**) to mice implanted human breast cancer tumors was confirmed by the above mentioned fluorescence-based imaging.

The other result that was obtained in these investigations was that tumor growth was completely suppressed by this combination (Fig. 16). In fact, HerGa not only prevented tumor growth but also appeared to reduce the size of the tumors that were already established at the time of treatment. The novel results of highly effective tumor-growth regression in mice were obtained with no detectable effect on off-target tissues such as the heart and the carrier protein displayed no immunogenicity. The dose needed for the latter purpose was exceedingly small (much lower than with doxorubicin, a leading anti-cancer drug) without side effects characteristic of other drugs, and without radiation as in photodynamic therapy. Significant tumor shrinkage by doxorubicin could only be observed if mice received relatively high doses (2.5 mg/kg) injected *intratumorally*, thus implying that *systemic* HerGa has similar effect to nearly 300 times higher doses of doxorubicin delivered *intratu-*

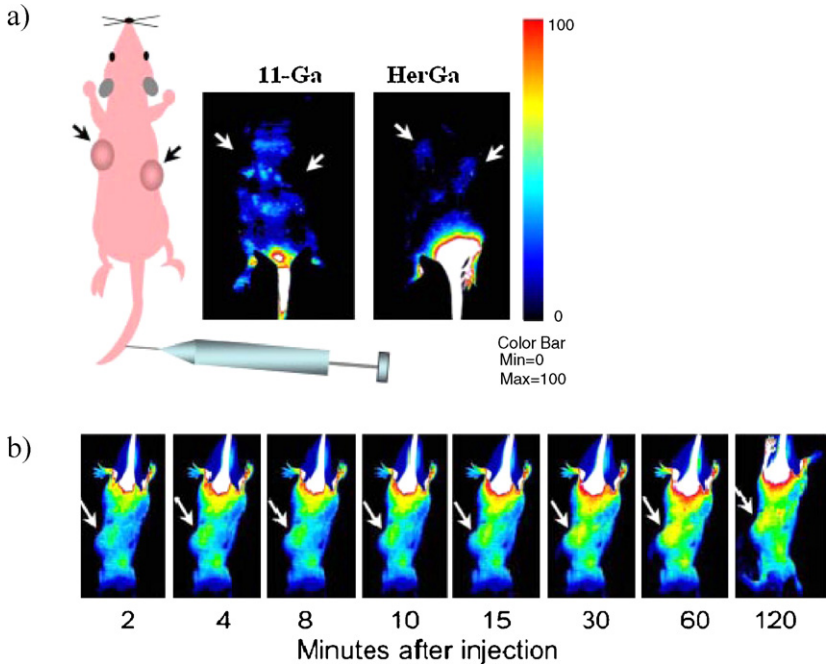

Fig. 15. (a) Fluorescence-based imaging of tumor upon injection of bio-conjugated **11-Ga** (HerGa) into breast cancer implanted mice. (b) Images taken at sequential time points after receiving HerGa via tail injection. The arrow points to the tumors. Figure was reproduced from Ref. [76], with permission of the copyright holders.

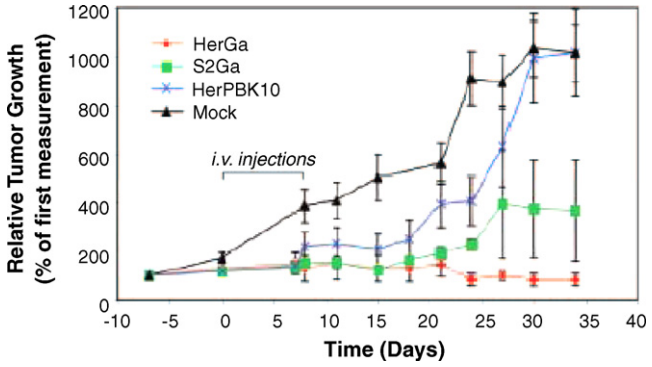

Fig. 16. Tumor volumes measured before, during, and after treatment. Mice were euthanized at 25 days after the last day of treatment, and tissues harvested for histological assessment. $n = 5–9$ tumors per treatment group. Figure was reproduced from Ref. [76], with permission of the copyright holders.

morally. The mechanism of action regarding tumor cell destruction by HerGa is not clear yet, but the advantage of being able to follow the biodistribution of an active drug in live animals is enormous.

10. Summary

Despite the apparent similarity of corroles and porphyrins, corroles display unique structural, spectroscopic, and photophysical properties that are not shared by porphyrins or any other metal-ligating molecules. The aim of this review was to provide a high quality understanding and appreciation of these features, which may serve as a guide for the design of tailor-made corroles for advanced applications. This task was fulfilled by a survey of investigations that focused on main group corroles. These complexes are easier to analyze because of the absence of interactions between unpaired metal d electrons and the corrole π system. We trust that the information provided in this review will be a significant asset for the steadily growing number of researchers who wish to take advantage of corroles in their fields of expertise.

Acknowledgements

We wish to thank our current collaborators: Harry Gray (Caltech), Daniel Farkas (Univ. S. California), Lali Medina-Kauwe (Cedars-Sinai Med. Center), Len Levin (Univ. of Montreal), Ron Steer (Univ. of Saskatchewan), Moussa Youdim (Technion Med. School), Mickey Aviram (Technion Med. School), Israel Goldberg (Tel-Aviv Univ.), Haim Levanon and Alex Berg (Hebrew Univ. of Jerusalem), for their contributions in the advancing of triarylcorrole chemistry from infancy to its current stage. Current financial support of the work on corroles is acknowledged as well, by: Technion V. P. R. funds, DFG, ISF, BSF, and the Herbert Irving Cancer and Atherosclerosis Research Fund. Last listed, but certainly most acknowledged, are the current students and coworkers at the Technion: Dr. Irena Saltsman, Dr. Atif Mahammed, Zoya Okun, Adi Haber, Izana Etinger, Lena Rabinovich, Dr. Anil Kumar, Jenya Vestfrid, and Oshri Blank, as well as to Josh Palmer (Caltech) and Sijia Dong (Univ. of Hong Kong).

References

[1] D. Dolphin (Ed.), The Porphyrins, vol. 1, Academic Press, New York, 1978 (ch. 1).
[2] For a historical perspective on corrole, see: E. Jones, R. Bonnett, Biogr. Mems. Fell. R. Soc. 30 (1984) 318.
[3] (a) A. Mahammed, H.B. Gray, A.E. Meier-Callahan, Z. Gross, J. Am. Chem. Soc. 125 (2003) 1162;
(b) B. Ramdhanie, J. Telser, A. Caneschi, L.N. Zakharov, A.L. Rheingold, D.P. Goldberg, J. Am. Chem. Soc. 126 (2004) 2515;
(c) J.P. Collman, M. Kaplum, R.A. Decréau, Dalton Trans. (2006) 554.
[4] J. Grodkowski, P. Neta, E. Fujita, A. Mahammed, L. Simkhovich, Z. Gross, J. Phys. Chem. A 106 (2002) 4772.
[5] (a) A.W. Johnson, I.T. Kay, Proc. Chem. Soc. London (1964) 89;
(b) A.W. Johnson, I.T. Kay, J. Chem. Soc. (1965) 1620;
(c) A.W. Johnson, I.T. Kay, Proc. R. Soc. London, Ser. A: Math. Phys. Sci. 288 (1965) 334.
[6] H.R. Harrison, O.J.R. Hodder, D.C. Hodgkin, J. Chem. Soc. B (1971) 640.
[7] (a) J.L. Sessler, S.J. Weghorn, Expanded, Contracted, & Isomeric Porphyrins, Tetrahedron Org. Chem. Series 15 (1997) 11–125, Pergamon, Oxford (ch. 2);
(b) R. Paolesse, in: K.M. Kadish, K.M. Smith, R. Guilard (Eds.), The Porphyrin Handbook, vol. 2, Academic Press, New York, 2000, pp. 201–232 (ch. 11);
(c) C. Erben, S. Will, K.M. Kadish, in: K.M. Kadish, K.M. Smith, R. Guilard (Eds.), The Porphyrin Handbook, vol. 2, Academic Press, New York, 2000, pp. 233–300 (ch. 12).

[8] (a) Z. Gross, N. Galili, I. Saltsman, Angew. Chem. Int. Ed. 38 (1999) 1427;
(b) Z. Gross, N. Galili, L. Simkhovich, I. Saltsman, M. Botoshsnsky, D. Blaser, R. Boese, I. Goldberg, Org. Lett. 1 (1999) 599;
(c) R. Paolesse, L. Jaquinod, D.J. Nurco, S. Mini, F. Sagone, T. Boschi, K.M. Smith, Chem. Commun. (1999) 1307.
[9] For recent reviews on triarylcorroles see:
(a) I. Aviv, Z. Gross, Chem. Commun. 20 (2007) 1987;
(b) I. Aviv, Z. Gross, Chem. Eur. J. 15 (2009) 8382;
(c) L. Flamigni, D.T. Gryko, Chem. Soc. Rev. 38 (2009) 1635;
(d) D.T. Gryko, J. Porphyrins Phthalocyanines 12 (2008) 906;
(e) S. Nardis, D. Monti, R. Paolesse, Mini-Rev. Org. Chem. 2 (2005) 355;
(f) R. Paolesse, Synlett 15 (2008) 2215;
(g) D.T. Gryko, Eur. J. Org. Chem. 11 (2002) 1735;
(h) Z. Gross, J. Biol. Inorg. Chem. 6 (2001) 733;
(i) Z. Gross, H.B. Gray, Adv. Synth. Catal. 346 (2004) 165;
(j) J.F.B. Barata, M.G.P.M.S. Neves, A.C. Tome, J.A.S. Cavaleiro, J. Porphyrins Phthalocyanines 13 (2009) 415.
[10] For reviews on the related triazocorroles (corrolazines), see:
(a) D.T. Gryko, J.P. Fox, D.P. Goldberg, J. Porphyrins Phthalocyanines 8 (2004) 1091;
(b) D.P. Goldberg, Acc. Chem. Res. 40 (2007) 626.
[11] For the first example of each of these applications, see:
(a) Z. Gross, L. Simkhovich, N. Galili, Chem. Commun. (1999) 599;
(b) D. Walker, S. Chappel, A. Mahammed, J.J. Weaver, B.S. Brunschwig, J.R. Winkler, H.B. Gray, A. Zaban, Z. Gross, J. Porphyrins Phthalocyanines 10 (2006) 1259;
(c) D. Aviezer, S. Cotton, M. David, A. Segev, N. Khaselev, N. Galili, Z. Gross, A. Yayon, Cancer Res. 60 (2000) 2973.
[12] I. Saltsman, I. Goldberg, Z. Gross, Tetrahedron Lett. 44 (2003) 5669.
[13] I. Saltsman, L. Simkhovich, Y.S. Balazs, I. Goldberg, Z. Gross, Inorg. Chim. Acta 357 (2004) 3038.
[14] S. Licoccia, R. Paolesse, E. Tassoni, F. Polizio, T. Boschi, J. Chem. Soc. Dalton Trans. (1995) 3617.
[15] I. Luobeznova, L. Simkhovich, I. Goldberg, Z. Gross, Eur. J. Inorg. Chem. (2004) 1724.
[16] C. Bruckner, C.A. Barta, R.P. Brinas, J.A.K. Bauer, Inorg. Chem. 42 (2003) 1673.
[17] J.H. Palmer, M.W. Day, A.D. Wilson, L.M. Henling, Z. Gross, H.B. Gray, J. Am. Chem. Soc. 130 (2008) 7786.
[18] I. Luobeznova, M. Raizman, I. Goldberg, Zeev Gross, Inorg. Chem. 45 (2006) 386.
[19] L. Wagnert, A. Berg, E. Stavitski, T. Berthold, G. Kothe, I. Goldberg, A. Mahammed, L. Simkhovich, Z. Gross, H. Levanon, Appl. Magn. Reson. 30 (2006) 591.
[20] S. Nardis, F. Mandoj, R. Paolesse, F.R. Fronczek, K.M. Smith, L. Prodi, M. Montalti, G. Battistini, Eur. J. Inorg. Chem. (2007) 2345.
[21] A.E. Meier-Callahan, H.B. Gray, Z. Gross, Inorg. Chem. 39 (2000) 3605.
[22] L. Simkhovich, N. Galili, I. Saltsman, I. Goldberg, Z. Gross, Inorg. Chem. 39 (2000) 2704.
[23] L. Simkhovich, I. Goldberg, Z. Gross, Inorg. Chem. 41 (2002) 5433.
[24] L. Simkhovich, A. Mahammed, I. Goldberg, Z. Gross, Chem. Eur. J. 7 (2001) 1041.
[25] L. Simkhovich, I. Luobeznova, I. Goldberg, Z. Gross, Chem. Eur. J. 9 (2003) 201.
[26] J. Bendix, H.B. Gray, G. Golubkov, Z. Gross, Chem. Commun. (2000) 1957.
[27] G. Golubkov, J. Bendix, H.B. Gray, A. Mahammed, I. Goldberg, A.J. DiBilio, Z. Gross, Angew. Chem. Int. Ed. 40 (2001) 2132.
[28] M. Bröring, C. Hell, C.D. Brandt, Chem. Commun. (2007) 1861.
[29] R.A. Eikey, S.I. Khan, M.M. Abu-Omar, Angew. Chem. Int. Ed. 41 (2002) 3591.
[30] L. Simkhovich, I. Goldberg, Z. Gross, J. Porphyrins Phthalocyanines 6 (2002) 439.
[31] L. Simkhovich, I. Goldberg, Z. Gross, Org. Lett. 5 (2003) 1241.
[32] A. Mahammed, I. Goldberg, Z. Gross, Org. Lett. 3 (2001) 3443.
[33] (a) C.M. Barzilay, S.A. Sibilia, T.G. Spiro, Z. Gross, Chem. Eur. J. 1 (1995) 222;
(b) N. Ehlinger, W.R. Scheidt, Inorg. Chem. 38 (1999) 1316;
(c) K.A. Nguyen, P.N. Day, R. Pachter, J. Phys. Chem. A 103 (1999) 9378.
[34] For a review on N-substituted porphyrins and corroles: A.H. Jackson, in: D. Dolphin (Ed.), The Porphyrins, Vol. I, Academic Press, New York, 1979 (chap 8).
[35] (a) Z. Gross, N. Galili, Angew. Chem. Int. Ed. 38 (1999) 2366;
(b) L. Simkhovich, P. Iyer, I. Goldberg, Z. Gross, Chem. Eur. J. 8 (2002) 2595.
[36] A. Ghosh, K. Jynge, Chem. Eur. J. 3 (1997) 823.
[37] L. Simkhovich, I. Goldberg, Z. Gross, J. Inorg. Biochem. 80 (2000) 235.
[38] J. Bendix, I.J. Dmochowski, H.B. Gray, A. Mahammed, L. Simkhovich, Z. Gross, Angew. Chem. Int. Ed. 39 (2000) 4048.
[39] (a) I. Saltsman, A. Mahammed, I. Goldberg, E. Tkachenko, M. Botoshansky, Z. Gross, J. Am. Chem. Soc. 124 (2002) 7411;
(b) J.J. Weaver, K. Sorasaenee, M. Sheikh, R. Goldschmidt, E. Tkachenko, Z. Gross, H.B. Gray, J. Porphyrins Phthalocyanines 8 (2004) 76.
[40] L. Wagnert, R. Rubin, A. Berg, A. Mahammed, Z. Gross, H. Levanon, J. Phys. Chem. B (2010), doi:10.1021/jp911465p.
[41] (a) R. Patra, A. Chaudhary, S. Kumar Ghosh, S. Prasad Rath, Inorg. Chem. 49 (2010) 2057;
(b) M.K. Safo, G.P. Gupta, F.A. Walker, W.R. Scheidt, J. Am. Chem. Soc. 113 (1991) 5497.
[42] A. Mahammed, I. Giladi, I. Goldberg, Z. Gross, Chem. Eur. J. 7 (2001) 4259.
[43] K. Sorasaeneea, P. Taqavia, L.M. Henlinga, H.B. Gray, E. Tkachenko, A. Mahammed, Z. Gross, J. Porphyrins Phthalocyanines 11 (2007) 189.
[44] A.E. Meier-Callahan, A.J. Di Bilio, L. Simkhovich, A. Mahammed, I. Goldberg, H.B. Gray, Z. Gross, Inorg. Chem. 40 (2001) 6788.
[45] J.H. Palmer, A. Mahammed, K.M. Lancaster, Z. Gross, H.B. Gray, Inorg. Chem. 48 (2009) 9308.
[46] R.K. Hocking, S. DeBeer George, Z. Gross, F.A. Walker, K.O. Hodgson, B. Hedman, E.I. Solomon, Inorg. Chem. 48 (2009) 1678.
[47] K.M. Kadish, Prog. Inorg. Chem. 34 (1986) 435.
[48] (a) Z. Gross, C. Barzilay, Angew. Chem. Int. Ed. Eng. 31 (1992) 1615;
(b) Z. Gross, C. Barzilay, Angew. Chem. 104 (1992) 1672.
[49] K.M. Kadish, Z. Ou, V.A. Adamian, R. Guilard, C.P. Gros, C. Erben, S. Will, E. Vogel, Inorg. Chem. 39 (2000) 5675.
[50] A. Mahammed, Z. Gross, J. Inorg. Biochem. 88 (2002) 305.
[51] Y.S. Balazs, I. Saltsman, A. Mahammed, E. Tkachenko, G. Golubkov, J. Levine, Z. Gross, Magn. Reson. Chem. 42 (2004) 624.
[52] D. Kowalska, X. Liu, U. Tripathy, A. Mahammed, Z. Gross, S. Hirayama, R.P. Steer, Inorg. Chem. 48 (2009) 2670.
[53] K.M. Kadish, S. Will, V.A. Adamian, B. Walther, C. Erben, Z. Ou, N. Guo, E. Vogel, Inorg. Chem. 37 (1998) 4573.
[54] A. Mahammed, Z. Gross, Dalton Trans. 39 (2010) 2998.
[55] Z. Gross, H.B. Gray, Comments Inorg. Chem. 27 (2006) 61.
[56] Z. Gross, A. Mahammed, J. Porphyrins Phthalocyanines 6 (2002) 553.
[57] M. Mastroianni, W. Zhu, M. Stefanelli, S. Nardis, F.R. Fronczek, K.M. Smith, Z. Ou, K.M. Kadish, R. Paolesse, Inorg. Chem. 47 (2008) 11680.
[58] K.M. Kadish, C. Erben, Z.P. Ou, V.A. Adamian, S. Will, E. Vogel, Inorg. Chem. 39 (2000) 3312.
[59] P.J. Brothers, Chem. Commun. (2008) 2090.
[60] (a) A.M. Albrett, J. Conradie, P.D.W. Boyd, G.R. Clark, A. Ghosh, P.J. Brothers, J. Am. Chem. Soc. 130 (2008) 2888;
(b) A.M. Albrett, J. Conradie, A. Ghosh, P.J. Brothers, Dalton Trans. (2008) 4464;
(c) A.M. Albrett, P.D.W. Boyd, G.R. Clark, E. Gonzalez, A. Ghosh, P.J. Brothers, Dalton Trans. 39 (2010) 4032.
[61] R. Paolesse, S. Nardis, M. Venanzi, M. Mastroianni, M. Russo, F.R. Fronczek, M.G.H. Vicente, Chem. Eur. J. 9 (2003) 1192.
[62] X. Liu, A. Mahammed, U. Tripathy, Z. Gross, R.P. Steer, Chem. Phys. Lett. 459 (2008) 113.
[63] A. Mahammed, J.J. Weaver, H.B. Gray, M. Abdelas, Z. Gross, Tetrahedron Lett. 44 (2003) 2077.
[64] See also, L.L. You, H. Shen, L. Shi, G.L. Zhang, H.Y. Liu, H. Wang, L.N. Ji, Sci. China Phys. Mech. Astron. 53 (2010) 1491.
[65] J.H. Palmer, A.C. Durrell, Z. Gross, J.R. Winkler, H.B. Gray, J. Am. Chem. Soc. 132 (2010) 9230.
[66] L. Wagnert, A. Berg, E. Stavitski, I. Luobeznova, Z. Gross, H. Levanon, J. Porphyrins Phthalocyanines 11 (2007) 645.
[67] A. Mahammed, H.B. Gray, J.J. Weaver, K. Sorasaenee, Z. Gross, Bioconjugate Chem. 15 (2004) 738.
[68] A. Mahammed, Z. Gross, J. Am. Chem. Soc. 127 (2005) 2883;
A. Mahammed, Z. Gross, Chem. Commun 46 (2010) 7040.
[69] P.A. Zunszain, J. Ghuman, T. Komatsu, E. Tsuchida, S. Curry, BMC Struct. Biol. 3 (2003) 6.
[70] A. Haber, H. Agadjanian, L.K. Medina-Kauwe, Z. Gross, J. Inorg. Biochem. 102 (2008) 446.
[71] H. Agadjanian, J.J. Weaver, A. Mahammed, A. Rentsendorj, S. Bass, J. Kim, I.J. Dmochowski, R. Margalit, H.B. Gray, Z. Gross, L.K. Medina-Kauwe, Pharm. Res. 23 (2006) 367.
[72] A. Mahammed, Z. Gross, Angew. Chem. Int. Ed. 45 (2006) 6544.
[73] M. Eckshtain, I. Zilbermann, A. Mahammed, I. Saltsman, Z. Okun, E. Maimon, H. Cohen, D. Meyersteinc, Z. Gross, Dalton Trans. (2009) 7879.
[74] Z. Okun, L. Kupershmidt, T. Amit, S. Mandel, O. Bar-Am, M.B.H. Youdim, Z. Gross, ACS Chem. Biol. 4 (2009) 910.
[75] J. Youn Hwang, H. Agadjanian, L.K. Medina-Kauwe, Z. Gross, H.B. Gray, K. Sorasaenee, D.L. Farkas, Prog. Biomed. Opt. Imaging 6859 (2008) 68590G.
[76] H. Agadjanian, J. Ma, A. Rentsendorj, V. Valluripalli, J.Y. Hwang, A. Mahammed, D.L. Farkas, H.B. Gray, Z. Gross, L.K. Medina-Kauwe, Proc. Natl. Acad. Sci. U.S.A. 106 (2009) 6105.